iScience

CellPress

Article

Cortical Correlates of Locomotor Muscle Synergy Activation in Humans: An Electroencephalographic Decoding Study

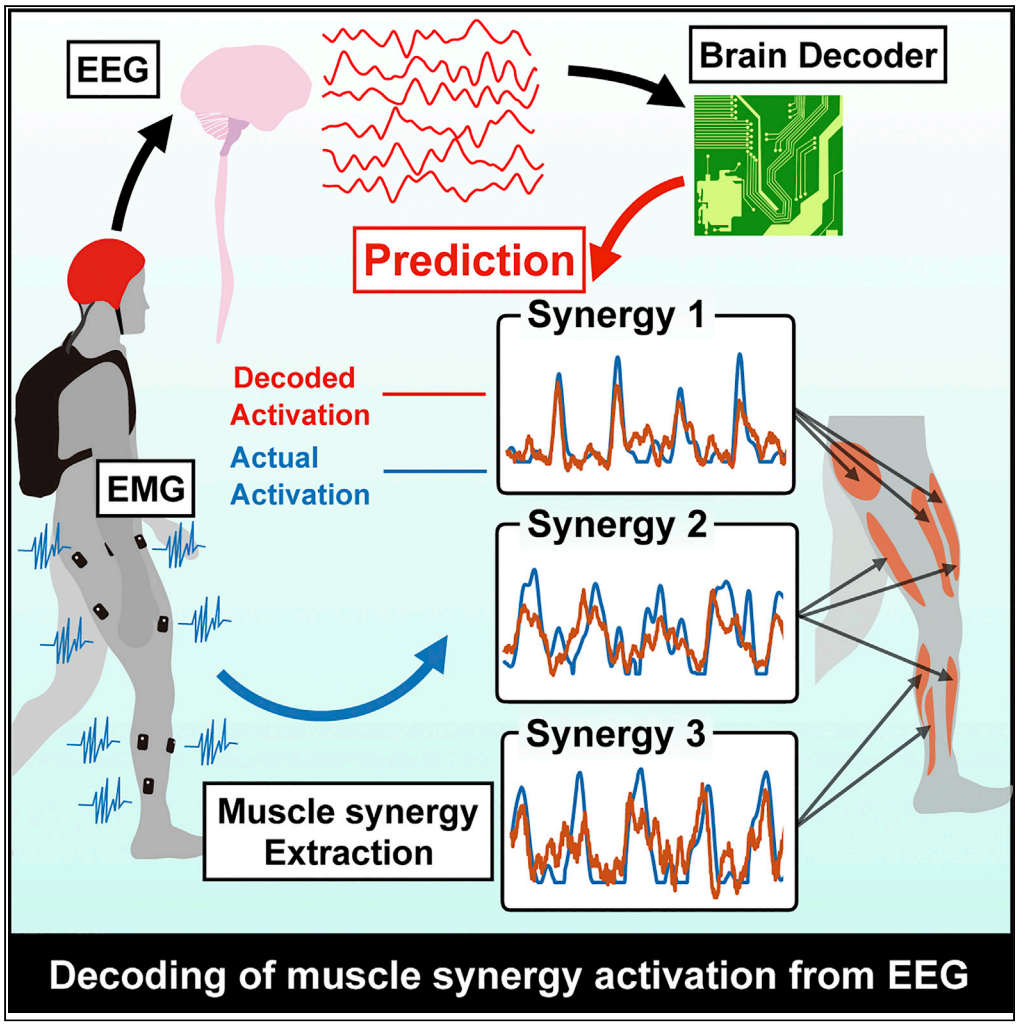

Hikaru Yokoyama, Naotsugu Kaneko, Tetsuya Ogawa, Noritaka Kawashima, Katsumi Watanabe, Kimitaka Nakazawa

nakazawa@idaten.c.u-tokyo.ac.jp

HIGHLIGHTS

We examined relationships of brain and locomotor muscle synergies by brain decoding

Locomotor muscle synergy activation was successfully decoded from EEG signals

Single muscle activation was decoded based on muscle-synergy-related EEG signals

The cortical correlates of locomotor muscle synergy may contribute to BMI for gait

Yokoyama et al., iScience *15*, 623–639
May 31, 2019 © 2019
https://doi.org/10.1016/j.isci.2019.04.008

iScience

CellPress

Article

Cortical Correlates of Locomotor Muscle Synergy Activation in Humans: An Electroencephalographic Decoding Study

Hikaru Yokoyama,[1,2] Naotsugu Kaneko,[3] Tetsuya Ogawa,[3] Noritaka Kawashima,[4] Katsumi Watanabe,[5,6,7] and Kimitaka Nakazawa[3,8,*]

SUMMARY

Muscular control during walking is believed to be simplified by the coactivation of muscles called *muscle synergies*. Although significant corticomuscular connectivity during walking has been reported, the level at which the cortical activity is involved in muscle activity (muscle synergy or individual muscle level) remains unclear. Here we examined cortical correlates of muscle activation during walking by brain decoding of activation of muscle synergies and individual muscles from electroencephalographic signals. We demonstrated that the activation of locomotor muscle synergies was decoded from slow cortical waves. In addition, the decoding accuracy for muscle synergies was greater than that for individual muscles and the decoding of individual muscle activation was based on muscle-synergy-related cortical information. These results indicate the cortical correlates of locomotor muscle synergy activation. These findings expand our understanding of the relationships between brain and locomotor muscle synergies and could accelerate the development of effective brain-machine interfaces for walking rehabilitation.

INTRODUCTION

Human locomotor movement is organized by the coordinated activation of a large number of muscles. It has been suggested that complex muscle activity is generated from a small number of groups of muscle activations called *muscle synergies* (d'Avella et al., 2003; Dominici et al., 2011; Ivanenko et al., 2004; Tresch et al., 1999; Yokoyama et al., 2016, 2017). Locomotor muscle synergies are thought to be structured in the spinal circuitry (Danner et al., 2015; McCrea and Rybak, 2008). Based on previous studies examining synergy activation among different subject groups, it has been suggested that the cortex activates locomotor muscle synergies (Danner et al., 2015; Dominici et al., 2011; Ivanenko et al., 2004). These studies reported that locomotor muscle synergy in healthy adults exhibited activation that was sharply timed around gait events (Ivanenko et al., 2004), whereas locomotor muscle synergy in neonates (Dominici et al., 2011) and patients with complete spinal cord injury (SCI) (Danner et al., 2015) exhibited smooth prolonged activation. The differences in the patterns in neonates and patients with SCI could be caused by immature and injured corticospinal pathways, respectively. Given that locomotor muscle synergies are thought to be structured in the spinal cord (Danner et al., 2015; McCrea and Rybak, 2008), the affected spinal locomotor output in patients with hereditary spastic paraplegia due to the degeneration of corticospinal fibers originating from the cortex (Martino et al., 2018) suggests cortical involvement in the activation of locomotor muscle synergies. Based on these findings, it is thought that cortical descending commands modulate basic locomotor muscle synergy activation generated by subcortical structures, particularly in the spinal cord. However, there is currently no direct evidence of cortico-muscle synergy relationships supported by simultaneous recordings of cortical activity and muscle synergy activation during walking.

Unlike quadruped animals (Armstrong, 1988; Drew et al., 2008), human bipedal walking is characterized by significant cortical activity even during undemanding steady-state walking (Artoni et al., 2017; Bradford et al., 2016; Bruijn et al., 2015; Gwin et al., 2011; La Fougere et al., 2010; Miyai et al., 2001; Petersen et al., 2012; Seeber et al., 2015; Wagner et al., 2012; Yang and Gorassini, 2006). Significant cortical activation has been demonstrated previously in premotor, supplementary motor, and primary sensorimotor regions during real and imagined walking using neuroimaging techniques such as positron emission tomography and near-infrared spectroscopy (La Fougere et al., 2010; Miyai et al., 2001). Recent studies using electroencephalography (EEG), which has greater temporal resolution, have demonstrated gait-phase-dependent

[1]Department of Electrical and Electronic Engineering, Tokyo University of Agriculture and Technology, Koganei-shi, Tokyo 184-8588, Japan

[2]Japan Society for the Promotion of Science, Chiyoda-ku, Tokyo 102-0083, Japan

[3]Department of Life Sciences, Graduate School of Arts and Sciences, The University of Tokyo, 3-8-1 Komaba, Meguro-ku, Tokyo 153-8902, Japan

[4]Department of Rehabilitation for the Movement Functions, Research Institute of National Rehabilitation Center for the Disabled, Tokorozawa-shi, Saitama 359-0042, Japan

[5]Faculty of Science and Engineering, Waseda University, Shinjuku-ku Tokyo 169-8555, Japan

[6]Art & Design, University of New South Wales, Sydney, NSW 2021, Australia

[7]Faculty of Kinesiology and Physical Education, University of Toronto, Toronto, ON M5S 1A1, Canada

[8]Lead Contact

*Correspondence: nakazawa@idaten.c.u-tokyo.ac.jp

https://doi.org/10.1016/j.isci.2019.04.008

This is an open access article under the CC BY-NC-ND license (http://creativecommons.org/licenses/by-nc-nd/4.0/).

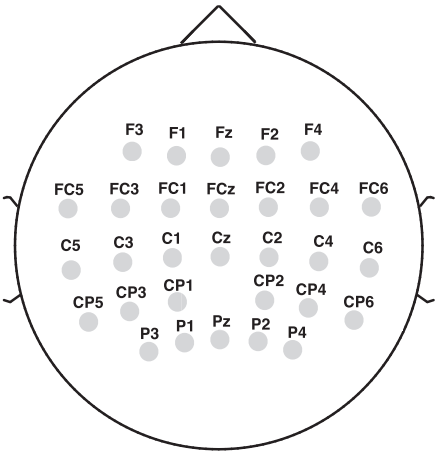

Figure 1. EEG Electrode Montage Corresponding to the International 10-20 System

Thirty electrode locations, which were used for the decoding analysis, are shown.

modulation of cortical activity, particularly in the sensorimotor cortex, using a combined method of independent component analysis and source localization techniques (Bradford et al., 2016; Bruijn et al., 2015; Gwin et al., 2011; Seeber et al., 2015; Wagner et al., 2012). Other EEG studies have demonstrated significant corticomuscular connectivity between the leg sensorimotor area and leg muscles during walking using individual muscle-level analysis (Artoni et al., 2017; Petersen et al., 2012). Although the results of these studies suggest strong relationships between cortical and muscle activity during walking, the level at which the cortical activity is related to muscle activity (at muscle synergies or individual muscles) remains unclear.

To address this question, we hypothesized that human cortical activity reflects muscle synergy activity more than individual muscle activity based on the above-mentioned possibility of cortical control of locomotor muscle synergy; we then examined how the cortex is involved in muscle activation during walking by decoding the activations of muscle synergies and individual muscles from EEG signals. Brain decoding techniques, which predict the mental or motor state of a human from recorded brain signals, have received substantial attention for the development of brain-machine interfaces (BMIs) for repairing or assisting deficits in cognitive or sensory motor functions (Lebedev and Nicolelis, 2006, 2017; Patil and Turner, 2008). In addition to potentially restoring lost functions, neural decoding can provide information on the physiological principles of how motor movements are controlled by the brain (Nicolelis, 2003).

In this study, using neural decoding techniques, we demonstrate that the activation of muscle synergies can be decoded from cortical activity and that the decoding accuracy for muscle synergies is greater than that for individual muscles. In addition, we show that the decoding of individual muscle activity is based on muscle-synergy-related cortical information. These results provide experimental evidence of the cortical correlates of locomotor muscle synergies in humans. In addition, they shed light on the relationships between brain activity and muscle synergies during walking and provide an important basis for developing effective neuroprostheses for walking rehabilitation.

RESULTS

Twelve healthy participants walked on a treadmill at 0.55 m/s for 7 min 30 s. Surface electromyographic (EMG) signals were recorded from 13 leg muscles on the right side. EEG signals were recorded from 63 channels. EEG data from 30 channels (Figure 1), which are assumed to be less affected by eye blinks and facial or cranial muscle activity, were used for subsequent analysis. Using the EMG and EEG signals, we tried to decode individual muscle and muscle synergy activations from cortical activity. See Figure 2 for an overview of our decoding methodology.

Extracted Locomotor Muscle Synergies

The recorded EMGs were rectified and smoothed by a low-pass filter. Next, using non-negative matrix factorization (NMF) (Clark et al., 2010; d'Avella and Bizzi, 2005; Dominici et al., 2011; Lee and Seung, 1999; Yokoyama et al., 2016), muscle synergies were extracted from each participant. From the low-pass filtered EMGs, 4.17 $\pm$ 0.58 (mean $\pm$ SD) muscle synergies were extracted from each participant.

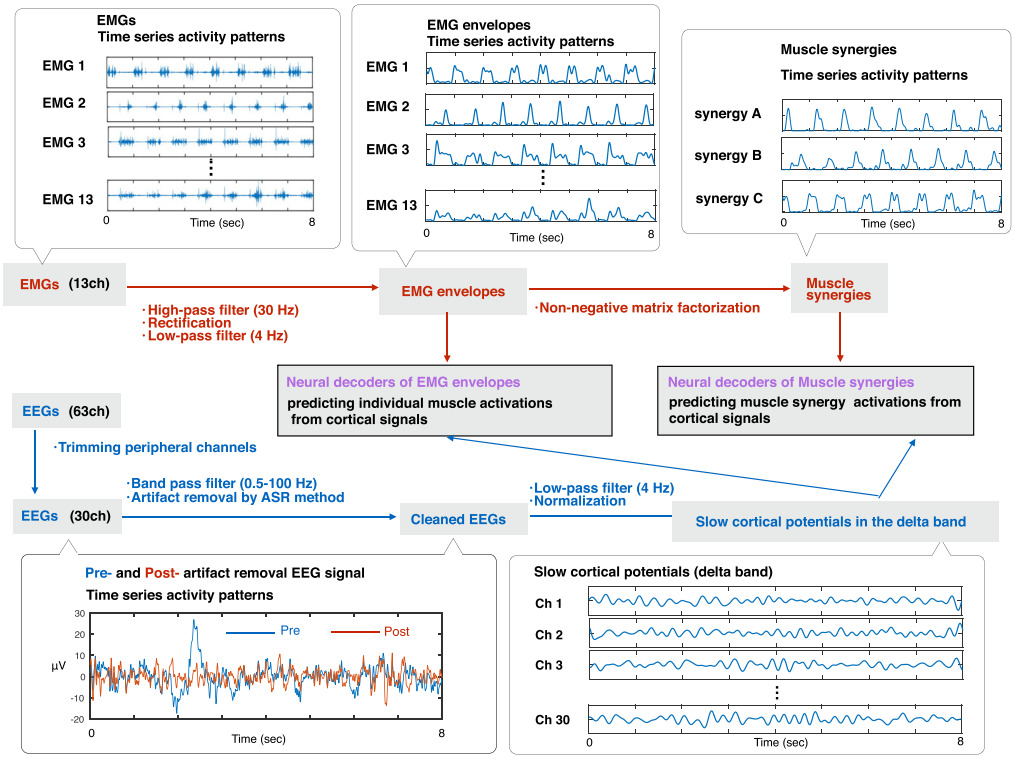

Figure 2. Schematic Diagram Depicting the Neural Decoding of Locomotor Muscle Synergy and Individual Muscle Activations from Simultaneously Recorded EEG Signals

Examples of 8 s of raw EMG signals, EMG envelopes, muscle synergies, pre- and postartifact removal EEG signal from an electrode, and slow cortical potentials in the delta band are shown.

The extracted muscle synergies were grouped into five types using cluster analysis (synergy A–E, Figure 3). Table S1 summarizes the characteristics of the extracted locomotor muscle synergies.

Neural Decoding of Activation of Muscle Synergies and Individual Muscles from EEG Signals

As preparation for neural decoding, recorded EEG signals were band-pass filtered in the delta band (0.5–4 Hz). The filtered non-rectified signals, which are called *slow cortical potentials*, were confirmed to be particularly informative for decoding motor-related parameters (Bradberry et al., 2010; Contreras-Vidal et al., 2018; Nakanishi et al., 2017; Presacco et al., 2011, 2012; Waldert et al., 2008). We used a time-embedded (10 lags, corresponding to 0–90 ms ahead of the muscle activation) linear model, also referred to as *Wiener filter*, to decode individual muscle and muscle synergy activations from the slow cortical potentials, as used in previous studies decoding motor parameters (Bradberry et al., 2010; Contreras-Vidal et al., 2018; Nakanishi et al., 2017; Presacco et al., 2011, 2012; Waldert et al., 2008).

Figure 4 provides examples of real and reconstructed muscle synergy activations (Figure 4A) and individual muscle activations (Figure 4B) from a participant. In this participant, all locomotor muscle synergy activations were successfully reconstructed based on visual inspection of the similarity between the real and reconstructed activations (Figure 4A). In contrast, in individual muscle activation, the amplitude modulation was not sufficiently reconstructed in some muscles, such as sartorius (SART), adductor magnus (AM), peroneus longus (PL), and soleus (SOL) (Figure 4B).

To quantify the decoding accuracy, we calculated the coefficient of determination (R^2) between the real and reconstructed activations in each decoder (Figure 5). The mean values across the participants ranged from 0.25 to 0.28 in muscle synergy decoders and from 0.11 to 0.28 in individual muscle decoders (Figure 5A). Although some individual muscles showed a similar decoding accuracy to that of muscle synergies (gluteus medius (Gmed), gluteus maximus (GM), biceps femoris (BF), SOL, and gastrocnemius medialis (MG); R^2 ranged from 0.24–0.28), the majority of individual muscles showed a lower decoding

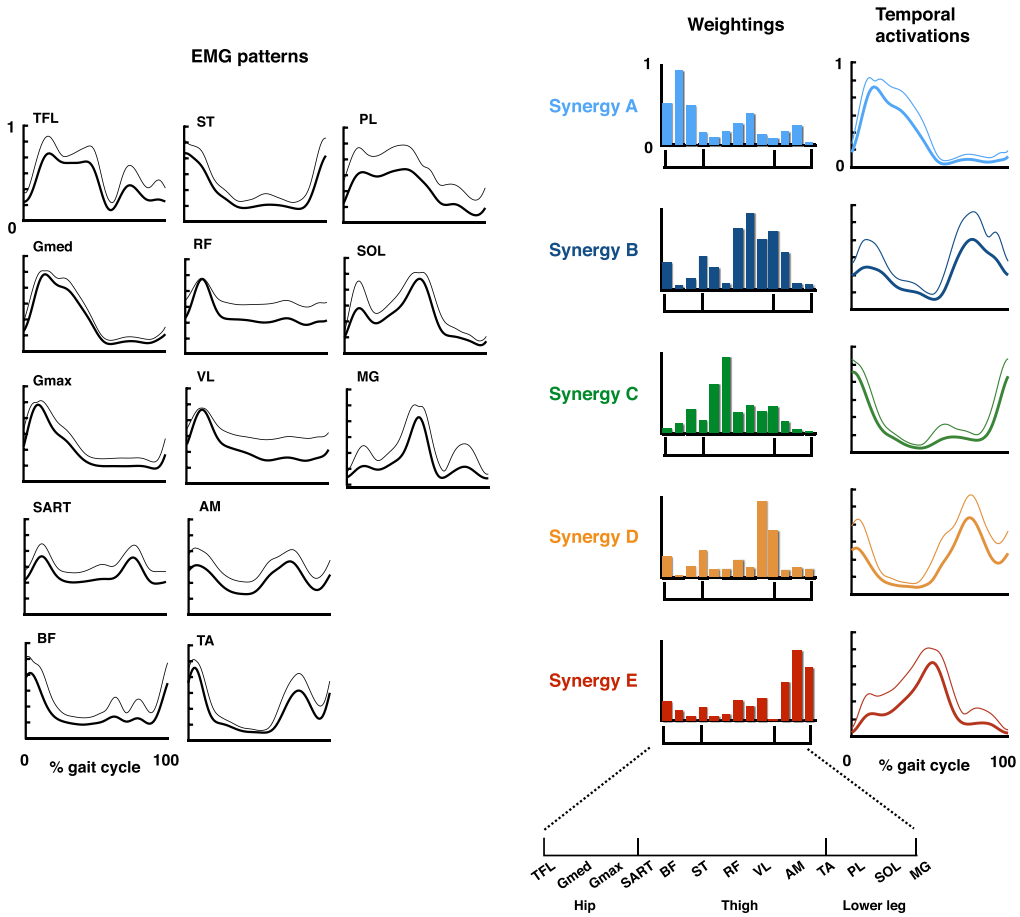

Figure 3. Muscle Activation Patterns and Extracted Locomotor Muscle Synergies

In the left part, black lines indicate the averaged muscle activation patterns across participants during a gait cycle. Thick lines indicate the average temporal activation patterns, whereas thin lines indicate the SDs. In the right part, five extracted types of locomotor muscle synergies are shown. Average muscle weightings (bars) and corresponding temporal activation patterns (waveforms) across participants in each type of locomotor muscle synergy are shown. Each bar height represents the relative level of activation of each muscle synergy. An enlarged view of the x axis is shown at the bottom. Lines indicate the temporal activation patterns of the muscle synergies. Thick lines indicate average temporal activation patterns, whereas thin lines indicate their SD. See also Table S1.

accuracy (R^2 ranged from 0.11–0.22). Regarding the general trend of differences in the accuracy between the two decoder types, the across-participant mean of the overall accuracy (i.e., averaged correlation values across all decoders in each type [muscle synergy or individual muscle]) of the muscle synergy decoder was higher than that of the individual muscle decoder ($t(11) = 4.42$, $p = 0.0001$, paired t test, Figure 5B).

To examine whether the difference in the overall decoding accuracy between the two types of decoders stemmed from differences in the number of decoders (individual muscles: 13, muscle synergies: 3–5 depending on participants) (Figure 5B), we calculated the overall decoding accuracy using the same number of randomly sampled individual muscle decoders with muscle synergies from 13 muscles. We iterated the procedure 10,000 times and calculated the 95% confidence interval of the distribution of the 10,000 values of the across-participant mean of the overall decoding accuracy of individual muscles (Figure S1). As a result, the participant mean of the overall decoding accuracy of muscle synergy decoders was larger than all the 10,000 values of the participant mean of the overall decoding accuracy of individual muscles (i.e., larger than the 95% confidence interval) (Figure S1). Thus the differences in the number of the two types of decoders did not affect the comparison results of the overall decoding accuracies with regard to the overall trend of the two decoder types.

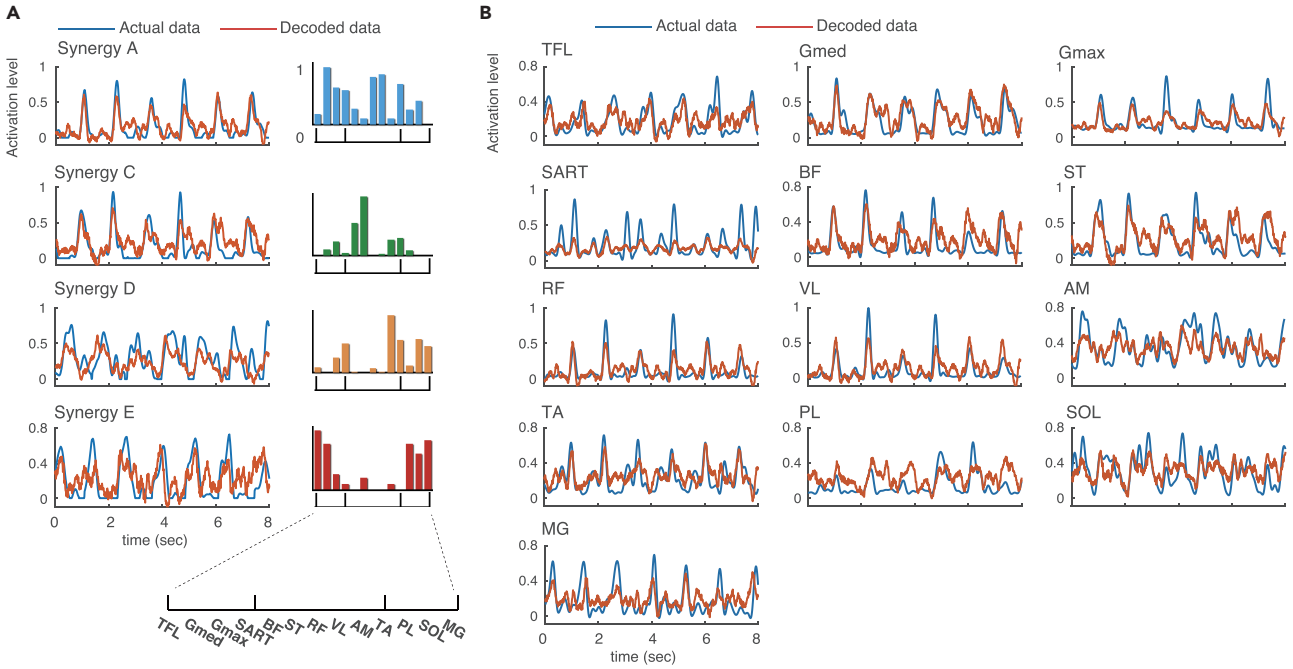

Figure 4. Typical Examples of Decoded and Actual Activations from a Participant

(A and B) Red and blue waveforms indicate decoded and actual activation patterns, respectively. (A) Muscle synergy activations are shown. Bars represent muscle synergy. (B) Individual muscle activations are shown.

Next, to validate the results of neural decoding, the same decoding process was performed on phase-randomized EEG signals to estimate the chance levels. After the phase randomization, the power spectrum was preserved in the surrogate data, but the phase relation to the muscle activity was disrupted. The time series EEG data throughout the recording duration were phase randomized. We generated 100 surrogate datasets and evaluated the mean and 95% confidence intervals of the decoding accuracy from the distribution of decoding accuracy of the surrogate datasets (Figure 5C). The decoding accuracy from the phase-randomized data was low regardless of the type of muscle synergies or individual muscles (range of mean R^2 values: 0.0067–0.012). At each decoder for each participant, the decoding accuracy from the original EEGs exceeded the 95% confidence interval of the surrogate datasets for all muscle synergy and individual muscle decoders in all the participants.

Relationships between Muscle Synergy Decoders and Individual Muscle Decoders

The decoding accuracy of muscle synergy activation was similar for all synergy types (Figure 5A). However, in individual muscle decoders, some muscles showed a similar decoding accuracy to that of muscle synergies, whereas the majority of individual muscles showed a lower decoding accuracy (Figure 5A). Namely, the decoding accuracy of individual muscle decoders varied widely across different muscles. In this study, it was assumed that cortical activity reflected muscle synergy activity more than individual muscle activity. Based on this assumption, the variability of decoding accuracy in individual muscles would be reproduced by individual muscle activations indirectly decoded from muscle synergy activations decoded from muscle synergy decoders. To test this hypothesis, we reconstructed individual muscle activations by summing the outputs of each decoded muscle synergy (Figure 6A). The decoding accuracy of directly decoded individual muscle activations was found to have a very strong positive correlation with that indirectly decoded from the outputs of decoded muscle synergies (r = 0.96, calculated from data from all participants, Figure 6B). This result indicates that if muscle activation is not well decoded through decoded muscle synergies, the decoding accuracy of the muscle will be low even when it is directly decoded.

The decoding accuracy relationships suggest that decoding of individual muscle activation is based on muscle-synergy-related cortical information. If so, the weights of the individual muscle decoders (W_{muscle}) should be represented as a linear combination of those of muscle synergy decoders (W_{syn}) with

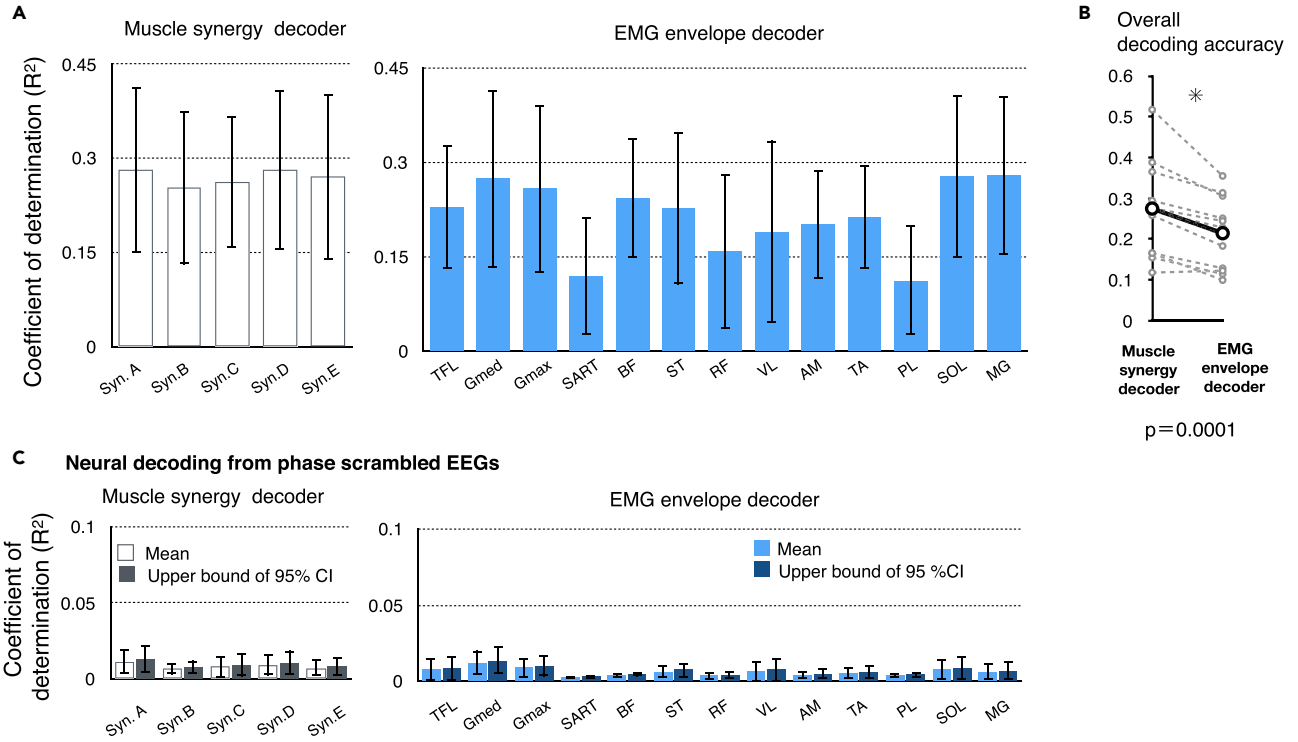

Figure 5. Decoding Accuracy of Activation of Muscle Synergies and Individual Muscles

(A) Decoding accuracy (coefficient of determination) for each muscle synergy type (left) and EMG envelope of an individual muscle (right). The mean and SD across participants are shown.

(B) Overall decoding accuracy for muscle synergy decoders and individual muscle decoders. Mean values across participants (black) and each participants' data (gray) are shown.

(C) Decoding accuracy when EEG phase was scrambled. The bars indicate the participant's mean of means and the upper ends of the 95% confidence interval obtained from the distribution of the surrogate datasets of EEG signals. The mean and SD across participants are shown.

See also Figures S1–S8 and Tables S7 and S8.

non-negative coefficients. To test this possibility, 300-dimensional weights (30 electrodes × 10 lags) of an individual muscle decoder were reconstructed as a linear combination of the weights of muscle synergy decoders with non-negative coefficients (W_{muscle}', conceptual schema presented in Figure 6C). The similarity between the original and reconstructed weights (i.e., W_{muscle} and W_{muscle}', respectively) was quantified by Pearson's correlation coefficient, which was 0.91 ± 0.11 (mean ± SD) across all muscles of all the participants. Regarding each type of muscle, the mean similarity values across participants ranged from 0.77 to 0.99 among muscles (Figure 6D). Thus, as expected, the weights of individual muscle decoders represented very similar patterns as those reconstructed from the weights of muscle synergy decoders.

Contributions of Electrodes to Neural Decoding

To evaluate the spatial contributions of cortical activity for predicting muscle synergy activations, we calculated the contribution of each electrode from the weights of the decoding model (Chao et al., 2010). Figure 7A shows examples of the contributions of each electrode to the decoding in one participant. In this participant, the contribution of each electrode was approximately 7% at the highest. Thus widely distributed cortical activity, rather than activity from one specific electrode and area, contributed to decoding. The widely distributed contribution of the whole cortex was also observed in the mean contribution in each type of synergy across participants (Figure 7B).

To further validate the widely distributed contribution of cortical activity to the decoding of locomotor muscle synergy, we divided the electrodes into four major regions of interest (ROIs), namely, frontal, central, lateral, and parietal ROIs (Figure 7C). Next, for each ROI, we performed the same decoding procedure used for all electrodes and compared the decoding accuracies. The comparisons of the decoding accuracy

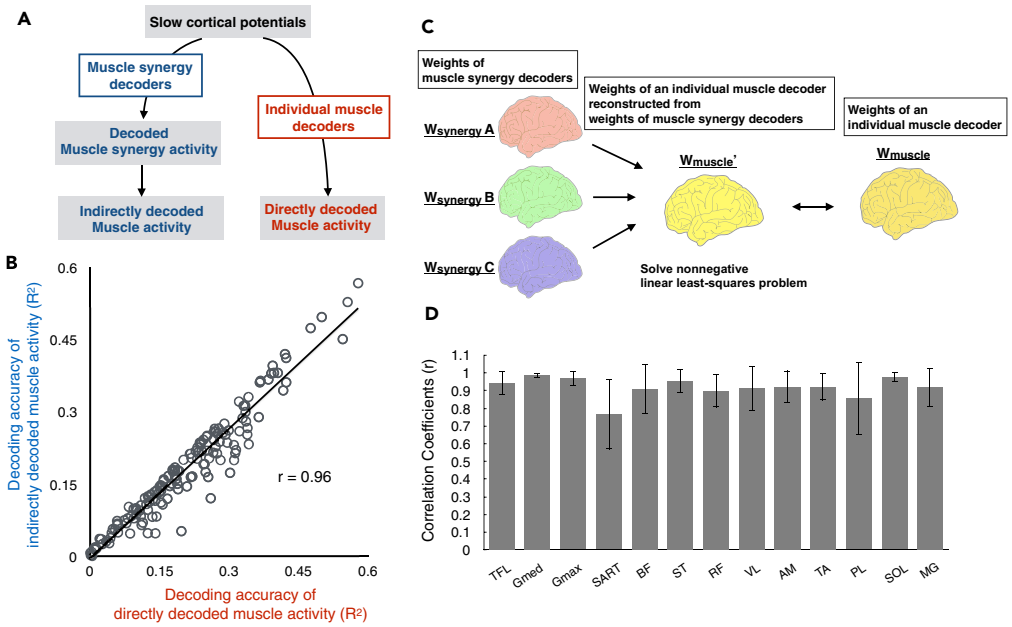

Figure 6. Relationships between Muscle Synergy Decoders and Individual Muscle Decoders

(A) A schematic flow diagram illustrating directly decoded muscle activity and indirectly decoded muscle activity reconstructed from decoded muscle synergies.

(B) Relationships of decoding accuracy in each individual muscle activity between those directly decoded from individual muscle decoders and those indirectly decoded from muscle synergy activations decoded from muscle synergy decoders. Values from all muscle synergies of all participants are plotted individually.

(C) Schematic diagram of reconstruction of weights of an individual muscle decoder from those of muscle synergy decoders.

(D) Similarity of weights of individual muscle decoders between the originals and those reconstructed from weights of muscle synergy decoders. The mean and SD across participants are shown.

did not show any significant differences among ROIs, except for that between the central and parietal ROIs in synergy E (Figure 7D). Nevertheless, the decoding accuracy in the full electrodes was significantly higher than that in each ROI (Figure 7D, $p < 0.05$, false discovery rate [FDR] corrected for multiple comparisons, see Tables S2–S6 for detailed statistical values). Interestingly, the mean decoding accuracy of the central ROI was the largest for all synergy types except synergy C, and significantly higher accuracy was found in the central ROI compared with frontal and parietal ROIs for synergy E (Figure 7D, $p = 0.023$ and 0.0082, respectively, FDR corrected for multiple comparisons).

Decoding of Muscle Synergy Activation Using EEG Signals in Different Time Lags

The above-mentioned results were obtained from decoders that use a negative time lag (−90 to 0 ms, forward model), as we were interested in examining the cortical descending control of muscle activity. In addition to the forward decoders, we attempted to decode using a positive (0–90 ms, backward model) and wider (−90 to 90 ms, wide time lag model) time lag. The across-participant means of the decoding accuracy (R^2) of the backward decoders ranged from approximately 0.25–0.29 among different muscle synergy types and were not significantly different from those of forward decoders in all muscle synergy types (Figure S2; see Table S7 for detailed statistical values). The wide time lag decoders showed a higher decoding accuracy (mean R^2 ranged from approximately 0.3–0.4) than both the other types of decoders in all muscle synergy types except synergy B (Figure S2). Thus both positive and negative time lag information were related to the activation of muscle synergy.

Effect of Normalization of EMG Amplitude on Decoding

Muscle activation levels vary across leg muscles during slow walking (Cappellini et al., 2006). Thus the normalization of EMG activity to the maximum for each muscle, which was used for the above-mentioned results, largely altered the relative amplitude across all the muscles. Therefore it is possible that the normalization affected the decoding of muscle synergy activation.

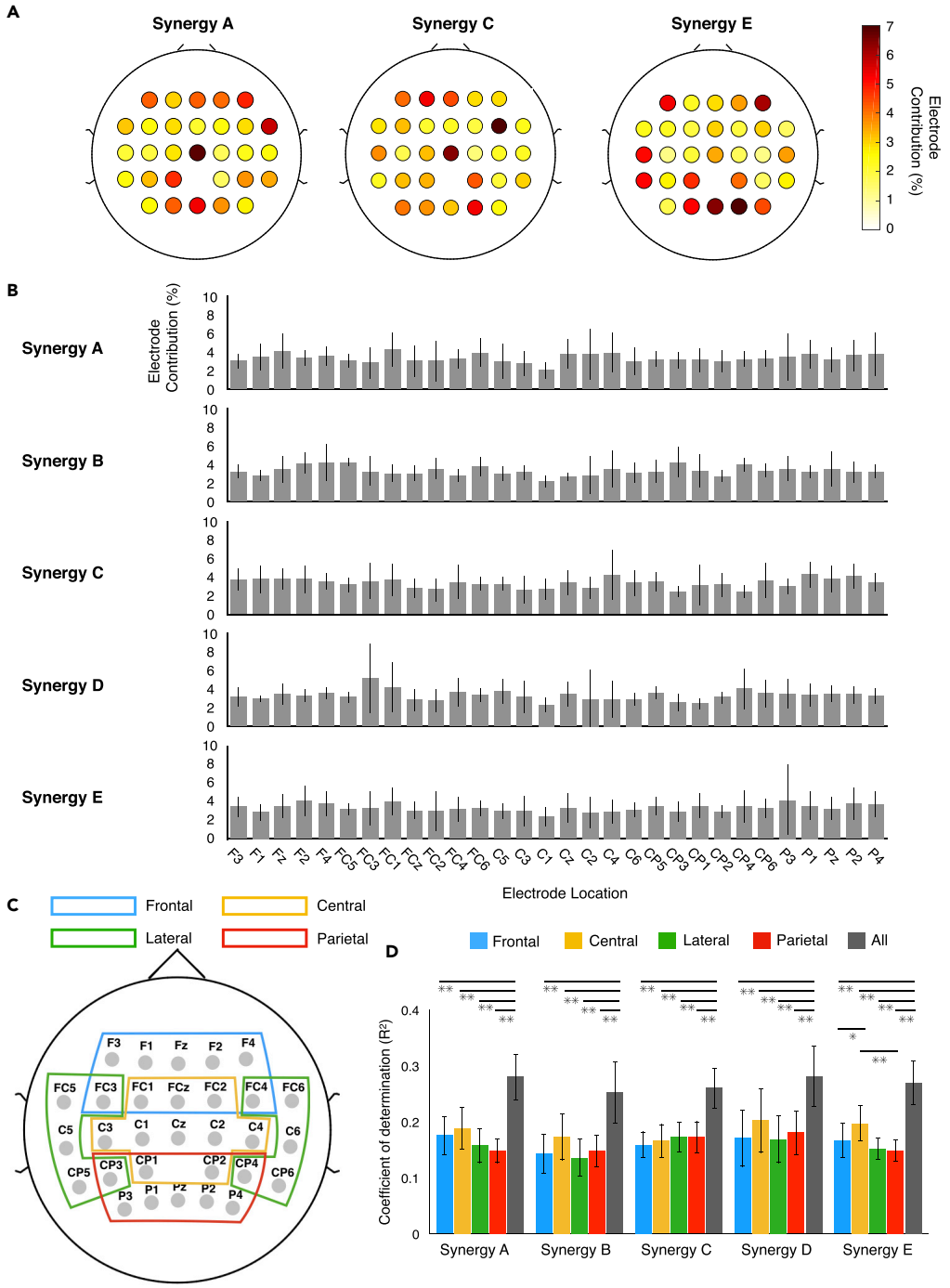

Figure 7. Contribution of Each Electrode to the Decoding of Muscle Synergy

(A–C) (A) Examples of contributions of each electrode to decoding from a participant. (B) Mean contribution of each electrode in each synergy type. The error bars indicate the SD. (C) Scalp map indicating the electrodes included in each ROI to examine the contributions from different cortical regions to decoding.

(D) Decoding accuracy by each ROI and all electrodes. Data are represented as mean ± SEM. Asterisks indicate significant differences (*$p < 0.05$, **$p < 0.01$, FDR corrected for multiple comparisons, See also Tables S2–S6 for detailed statistical values).

See also Figures S4–S9 and Tables S2–S6 and S8.

To examine the effect of the normalization on the decoding of muscle synergy activation we extracted muscle synergies from non-normalized EMG activity and performed a decoding analysis using the muscle synergy activation extracted from the non-normalized EMG. Five types of muscle synergies were extracted (Figure S3A), and the across-participant means of the decoding accuracy (R^2) ranged from approximately 0.20 to 0.27 among different muscle synergy types (Figure S3B). The decoding accuracy was comparable to those of the normalized muscle synergy activation (Figure 5, mean R^2 ranged from approximately 0.25–0.28), indicating that the EMG normalization did not largely affect our decoding results.

Effect of Motion Artifact on the Decoding

The potential effects of movement artifacts should be considered when recording EEGs during dynamic movements. Because the power spectra of EEGs, which are affected by motion artifact during walking, exhibit power peaks at the stride and step frequencies due to head motion (Arad et al., 2018; Kline et al., 2015; Nathan and Contreras-Vidal, 2016) we examined the power spectra of the EEGs using the fast Fourier transform. Figure S4 shows examples of EEG data at three electrodes (Cz, Pz, C6) for the diversity of their spatial localizations (top, back, and right side of the head, respectively) from participants who showed the best, moderate, and worst decoding accuracies—which were participants ID-6, ID-1, and ID-4, respectively. In these examples, one electrode (Cz of ID-6) showed an obvious high power at the step frequency. Regarding the other electrodes, although the power spectra in some electrodes showed peaks at the stride and step frequencies, the amplitudes were comparable with the maximum power in other frequencies in the delta band (0.5–4.0 Hz).

Because obviously large peaks in the movement frequency, when compared with the power in the other frequencies like Cz of ID-6, have been previously demonstrated to be a feature of motion artifacts in EEGs during walking (Castermans et al., 2014; Kline et al., 2015), such electrodes would have been affected by movement artifact. Therefore we calculated the relative power between the peak power in frequency from the stride frequency to the step frequency and the mean power in the delta band frequency (0.5–4.0 Hz) as a rough indicator of the artifact size of each electrode. Then the correlation between the artifact size and electrode contribution to the decoding was calculated. If the decoding was based on movement artifact, the EEG signals with a large artifact size, which were assumed to greatly reflect motion artifacts less buried by cortical activity, were highly weighted in the decoder model; thus the correlation would exhibit a significantly positive value. Figure S5 shows scatterplots of the artifact size and electrode contribution from the three participants presented in Figure S4. It is noteworthy that the most contributing electrode showed lower artifact size in each decoder in Figure S5. In all participants, there was no significant positive correlation between the artifact size and electrode contribution, except for 2 of 54 decoders (Figure S6). These results suggest that the effect of motion artifact on the decoding was small.

Relationships between Head Acceleration and Slow Cortical Potentials

To further examine the effect of movement artifact on the decoding, we conducted a supplemental experiment by measuring head movement accelerations, as movement artifacts are mainly caused by vertical head accelerations (Kline et al., 2015). We measured triaxial head accelerations in addition to EEG and EMG signals from three healthy participants during walking on a treadmill under the same experimental and data-recording conditions used in the main experiment.

The overall decoding accuracies of the muscle synergies in each of the three participants were R^2 = 0.29, 0.21, and 0.20, respectively (Table S8). In the three participants, all head accelerations showed clear cyclic patterns (Figure S7). If the head acceleration affected the activation patterns of the slow cortical potentials, the two signals would show a correlation with a time lag, where the head movement precedes the slow cortical potentials. Because movement artifacts are mainly caused by vertical head accelerations (Kline et al., 2015), we examined the relationships between the vertical head acceleration time series and the slow cortical potentials at each electrode using cross-correlation (Figure S8A). In one participant (ID-S1), the correlation values were very low ($r < 0.06$ in all electrodes). In the other two participants (ID-S2 and ID-S3), the majority of electrodes showed almost no correlation ($r < 0.2$). Although some electrodes showed weak correlation (r ranged from about 0.2 to 0.3), the time lags varied greatly, and half of them indicated that EEG signals preceded the head accelerations. Given the high variability in the time lags, the weak correlation may indicate that the acceleration was not correlated with movement artifact, but instead with gait-phase-related cyclic brain activity in the EEG signals. In addition, there was no significant correlation between the maximum correlation value of the cross-correlation analysis and the

electrode contribution to decoding in all muscle synergy decoders in all participants (Figure S8B). Taken together, these results suggest that motion artifact derived from head acceleration has little effect on the decoding.

DISCUSSION

Cortical Correlates of Muscle Synergy Activation during Walking

The last 15 years of research has suggested that cortical descending commands modulate basic locomotor muscle synergy activation generated by subcortical structures (Clark et al., 2010; Danner et al., 2015; Dominici et al., 2011; Ivanenko et al., 2004). Nevertheless, currently, there has been no evidence of cortical correlates of locomotor muscle synergies from simultaneously recorded cortical and muscle activity. In this study, we revealed that activation of locomotor muscle synergies decoded from EEGs was moderately correlated with real activation (Figure 5A). Although some individual muscles showed a similar decoding accuracy to that of muscle synergies, the majority of individual muscles showed a lower decoding accuracy (Figure 5A). Regarding the general trend of differences between the two decoder types, mean decoding accuracy across all muscle synergy types were significantly higher than that of individual muscles (Figure 5B). By examining the relationships between individual muscle and muscle synergy decoders, we also showed that both types of decoders were based on almost the same cortical information (Figures 6B and 6D). Assuming that cortical activity encodes muscle synergy activation and both types of decoders are based on synergy-related cortical information, the following are considered as explanations for the differences in the decoding accuracies among the decoders: (1) all muscle synergies, which were strongly associated with synergy-related cortical information, were well decoded; (2) some individual muscles, which would be strongly associated with synergy-related cortical information, were well decoded, whereas other individual muscles, which would not be associated with synergy-related cortical information, were not well decoded. Given that decoding accuracy in muscle synergies are generally higher than in individual muscles, and the high possibility of contribution of synergy-related cortical information to both types of decoders, the decoding results demonstrate significant cortico-muscle synergy relationships during walking. Thus the present findings possibly support the hypothesis that the human cortex hierarchically controls locomotor muscle activity through muscle synergies rather than by directly controlling each muscle (Ting et al., 2015).

However, it should be kept in mind that it is difficult to examine causal relationships from cortical activity to muscle synergy activity, such as descending control of muscle synergies, using the decoding method in this study. It is highly possible that the cortical correlates of muscle synergies, which was demonstrated by the neural decoding in this study, stemmed not only from the descending commands but also from sensory-related cortical activity, including somatosensory, vestibular, and visual inputs. Given the task in this study (steady-state walking), somatosensory inputs originating from dynamic limb movements were probably dominant sensory inputs, which may have affected the decoding. Because the primary somatosensory cortex (S1) has a close link with the primary motor cortex (M1), as demonstrated by anatomical (Donoghue and Wise, 1982; Veinante and Deschênes, 2003) and functional (Witham et al., 2007) connectivity in animals, somatosensory inputs influence the cortical motor output in humans (Rosenkranz and Rothwell, 2004; Roy and Gorassini, 2008; Schabrun et al., 2012). Thus it is possible that the somatosensory inputs contributing to the decoding were not only communicating current bodily states but also indirectly involved in the control of locomotor muscle synergies through the sensorimotor network. In fact, a control framework has been proposed, where sensory information, including somatosensory inputs, contributes to the modification of muscle synergy activity through M1 during challenging walking tasks in cats based on physiological evidence (Drew and Marigold, 2015). Although the sensory contribution of muscle synergy control is limited to challenging walking conditions in cats, such sensory information might contribute to the control of locomotor muscle synergies during walking in humans given the significant brain to muscle connectivity, even during steady-state walking in humans unlike cats (Artoni et al., 2017).

Regarding the effects of neurological disorders on the locomotor muscle synergies, it was reported that patients with stroke recruit fewer locomotor muscle synergies as a result of the merging of healthy muscle synergies, which reflect disruption in the corticospinal descending pathways (Clark et al., 2010). Therefore poststroke changes suggest cortical involvement in the activation of the locomotor muscle synergies. Other evidence regarding the cortical control of locomotor muscle synergies has been suggested by altered activation of the muscle synergies in patients with complete SCI (Danner et al., 2015) and neonates

(Dominici et al., 2011). Both subject groups exhibited smooth sinusoidal-like activation patterns of locomotor muscle synergies rather than sharply timed activation, which was observed in healthy subjects (Ivanenko et al., 2004; Yokoyama et al., 2016). The sinusoidal-like activation patterns were also observed in other mammals (Dominici et al., 2011). Based on lack of corticospinal interactions in patients with SCI and neonates, this similarity may suggest that the sinusoidal-like activation patterns are phylogenetically conserved in the spinal circuits. Taken together, it is possible that cortical descending commands modulate basic locomotor muscle synergy activation patterns generated by the spinal cord into the sophisticated patterns underlying human-specific upright bipedal walking.

The decoded muscle synergy activation observed here was able to account for about 25% of the data variance of the actual activation, which implies that 75% was not accounted for (Figure 5). The not-so-high decoding accuracy is thought to be caused by a low signal-to-noise ratio (SNR) of EEG signals. Because EEG sensors are placed around the scalp—distant from the signal sources in the brain—the cortical signal is weak relative to various artifacts, such as electromagnetic, thermal, and mechanical noise. Therefore, in general, the SNR of EEGs is very low compared with those of invasive recording methods, such as electrocorticography (ECoG) and single-unit activity (SUA) (Ball et al., 2009a). In the present study, because the decoders attempted to extract meaningful activity from the signals with a low SNR, the decoding accuracy would not have been high. Another possible explanation for the low decoding accuracy is the partial contribution of the cortex to generate activation patterns of locomotor muscle synergies. Muscle synergy is considered to be recruited via multiple neural pathways via the brainstem and spinal cord, in addition to the cortex (Chvatal and Ting, 2012; Saltiel et al., 2015; Ting et al., 2015). Basic rhythmic activation patterns of locomotor muscle synergies are generated from the spinal cord itself (Danner et al., 2015). In addition, locomotor muscle synergy activation is modulated in response to afferent feedback during walking at latencies corresponding to long-latency responses (~100 ms), which are considered to be mediated by brainstem pathways (Chvatal and Ting, 2012). Therefore although the cortex is likely to be involved in the control of locomotor muscle synergies, its contribution may not be exclusively dominant. The partial contribution of the cortex to the control of locomotor muscle synergies may explain the not-so-high decoding accuracy observed in this study.

It is possible that the higher decoding accuracies of muscle synergies, compared with individual muscles, was a consequence of the fact that the muscle synergies represent a gait event in a gait cycle robustly among strides. However, although individual muscle activity represents a gait event weakly among strides, if the activity of cortical neurons highly co-varies with the muscle activity among the strides, the decoding accuracy of the individual muscle would be higher than that of muscle synergies. Therefore more robust muscle activity among strides does not necessarily mean its decoder has a higher decoding accuracy. Regarding the robustness of the representation of the phases of gait, it was reported that stride-to-stride variability of EMG patterns varies among lower limb muscles during walking (Winter and Yack, 1987). Because a muscle synergy is extracted to reconstruct activation of multiple muscles (maybe including muscles showing low and high stride-to-stride variability), muscle synergies may not necessarily be better at representing the phases of gait than single muscles. Because leg muscles can be selectively activated through spinal reflex circuits, even between synergistic muscles in both the lower leg (Duysens et al., 1991) and thigh (Kim et al., 1995) muscles, such subcortical adjustments of single muscle activity may be related to the lower decoding accuracies from the cortical signals in individual muscle decoders.

Spatially Global Cortical Contribution to the Decoding

Although activations of unilateral (right-sided) muscle synergies were decoded, widely distributed bilateral cortical activity, rather than activity from a specific electrode or area, contributed to the decoding (Figure 7). EEG records the electrical activity of the brain on the scalp through tissues, such as spinal fluid, bone, and skin. Because the bone has very low electrical conductivity, the electrical activity attenuates greatly and spreads widely on the scalp. Given the low spatial resolution of EEG, a possible reason for the bilateral widely distributed cortical contribution may be that the electrodes on the right side may have recorded the activity from the left-sided leg region of the primary motor cortex, as the leg motor area is located close to the midline. Another possibility is that the inner part of the primary motor cortex, which is folded in the longitudinal fissure of the cerebrum, corresponds to the thigh and lower leg region. Because neuron columns are perpendicular to the cortical surface (Asanuma, 1975), many axons of

neurons in the longitudinal fissure of the cerebrum are directed horizontally (left-right direction). Thus the electric field of such a horizontal cortical column (horizontal current source) spreads in the left-right direction (the schema is illustrated in Figure S9), and the peak amplitude is observed not directly above the tangential source, but rather at a distance of 2–5 cm along the scalp—depending on the depth of such a horizontal source (Srinivasan, 1999). Therefore unilateral leg muscle activity would be related to EEG signals in the bilateral cortices. As possible characteristics of muscle synergies related to the spatially global cortical contribution, a previous study showed that each locomotor muscle synergy activates bilateral leg muscles at a certain timing (Maclellan et al., 2014). In addition, Cappellini et al. (2006) showed that locomotor synergies activate the upper and lower limb muscles together. Therefore it is possible that muscle synergies extracted from unilateral muscle activity in the present study would have been part of muscle synergies at the level of whole body; thus spatially global cortical regions may have contributed to the decoding of the unilateral muscle synergies. In addition, a previous study showed that unilateral motor cortical regions, which encode muscle synergies of the leg and pelvic floor muscles, have functional connectivity with wide cortical regions including the contralateral cortex (Rana et al., 2015). The spatially wide functional networks might have contributed to the decoding of muscle synergy activation in the present study.

As with our results, previous studies of neural decoding while walking demonstrated that leg kinematics could be decoded from cortical signals from widely distributed regions (Presacco et al., 2011, 2012). Previous work has shown the contributions of widespread cortical circuits, including the posterior parietal cortex, motor cortex, somatosensory cortex, and visual cortex, to visually guided walking in cats (Drew and Marigold, 2015). Although the contribution of widespread cortical circuits is limited to challenging walking conditions in cats, such circuits may contribute to the control of human walking even during steady-state walking because the mechanical instability of human-specific bipedal walking (Kuo, 1999) requires additional cortical involvement. Indeed, widespread cortical activity has been reported during human walking by source estimation of EEG signals (Bulea et al., 2015; Gwin et al., 2011). In addition, motor imagery studies have demonstrated locomotor-related activity in brain regions including the primary and supplementary motor cortex and several bilateral parietal and frontal regions using functional magnetic resonance imaging (Van Der Meulen et al., 2014; Wang et al., 2008). Thus it is possible that locomotor-related global activity in the cortex can explain the widely distributed contribution of electrodes to the decoding of locomotor muscle synergy activations in the present study.

Although our results based on EEG measurements showed that spatially broad cortical activity contributed to the decoding, previous animal studies, which used more precise recording methods such as local field potentials and SUA, showed a solid association between motor cortical areas and muscle control during walking (Armstrong and Drew, 1984; DiGiovanna et al., 2016). In humans, ECoG studies have demonstrated the involvement of specific areas of the sensorimotor cortex in arm-reaching movements (Acharya et al., 2010; Ball et al., 2009b). Therefore it is important to keep in mind that the low spatial resolution of EEGs possibly affected the global cortical contribution in the decoding; thus other electrophysiological recording methods with a higher spatial resolution would provide a more precise spatial localization of cortical areas related to muscle synergy control in human walking.

Roles of Slow Cortical Potentials in Sensorimotor Control

In the present study, slow cortical potentials in the delta band (0.5–4 Hz) were used for our neural decoding method. Although such low-frequency cortical activity is associated with sleep (Hobson and Pace-Schott, 2002), recent studies suggest that low-frequency cortical activity contains sensorimotor-related information. For example, delta band cortical activity plays a role in decision making about somatosensory discrimination (Nácher et al., 2013) and prediction of sensory events (Saleh et al., 2010). In addition, neural decoding studies in humans have demonstrated that delta band activity is particularly informative for decoding kinematic parameters (Bradberry et al., 2010; Contreras-Vidal et al., 2018; Nakanishi et al., 2017; Presacco et al., 2011, 2012; Waldert et al., 2008) and muscle activity (Nakanishi et al., 2017). In recent rodent studies, multisensory integration in widespread brain networks through slow cortical waves was suggested by calcium imaging (Kuroki et al., 2018). As more direct evidence, a study on monkeys revealed intrinsic cyclic activity of slow cortical waves, functioning much like a spinal central pattern generator for locomotion, in the motor cortex and that slow waves synchronized upper-limb movements and muscle activity (Hall et al., 2014). In addition, they demonstrated the slow cortical dynamics during sleep and under sedation. Given the task commonality between upper-limb movement and sleep, it is possible that the slow cortical

dynamics are shared with walking. If the above-mentioned roles of slow cortical waves are conserved in humans, slow cortical waves may integrate muscle-synergy-related sensor information and be synchronized to muscle synergy activations. Therefore locomotor muscle synergy activations could be decoded from slow waves in this study.

Applicability to Brain-Machine Interfaces

The decoding methodology and results of this study could contribute to the development of more effective locomotor rehabilitation approaches for patients with neural disorders. Several recent studies have used a binary neural decoder to detect patients' intention to walk (i.e., "walk" or "idle") to support their walking movement (Donati et al., 2016; King et al., 2015). Unlike such binary decoders, our continuous decoders predict muscle activity changes with every moment and thus have the potential to develop a more precise gait supporting system. Recently, BMI systems, which control stimulators that activate muscles through functional electrical stimulation (FES) based on cortical signals, have been used to aid recovery of movement in impaired patients (Bouton et al., 2016). As a new stimulation pattern of FES, muscle synergy-based stimulation patterns have been suggested for upper-limb reaching (Muceli et al., 2010) and locomotion (Alibeji et al., 2015). The present results indicate that EEG signals contain information about the control of locomotor muscle synergies, providing fundamental information for effective neuroprosthetic systems based on a combined approach (e.g., BMI-FES with muscle-synergy-based stimulation patterns) for restoring locomotion. In addition to supporting impaired movement, both BMI (Donati et al., 2016) and FES (Everaert et al., 2010) can induce neural plasticity through long-term training. Therefore the BMI-FES system, based on muscle synergy decoders, would have the potential to greatly accelerate neural plasticity to enhance the functional recovery of walking.

Effects of Motion Artifacts on the Decoding

Although EEG is a suitable method for examining brain activity during walking because of its high temporal resolution and mobility, the potential effects of movement artifacts should be considered. The power spectra of EEGs, which are affected by motion artifact in walking, exhibit power peaks at the stride and step frequencies due to head motion (Arad et al., 2018; Kline et al., 2015; Nathan and Contreras-Vidal, 2016). Thus if our decoding results were based on motion artifact, the EEG electrodes, which showed a larger peak power in the movement frequencies and were assumed to reflect motion artifacts less buried by cortical activity, would highly contribute to the decoding. Nevertheless, there is almost no correlation between the size of peak power in the movement frequencies and electrode contribution (Figures S5 and S6). Rather, most contributing electrodes in each decoder showed a lower peak power in the movement frequencies (Figure S5). In addition, our supplemental experiment showed that head accelerations do not contribute to the decoding under the slow walking speed (0.55 m/s) (Figures S7 and S8), suggesting that motion artifact derived from head acceleration has little effect on the decoding results in the present study.

Some electrodes showed a peak power in the movement frequencies at a comparable amplitude to the maximum power in the other frequencies in the delta band (0.5–4.0 Hz) (Figure S4). Previous studies showed that rhythmic sensory inputs (Giabbiconi et al., 2004) and the observation of rhythmic movement (Kline et al., 2016) elicit a peak in the power spectra of EEGs at the given frequency. Given the knowledge of activity modulation of cortical neurons within a gait cycle in cats (Armstrong and Drew, 1984) and mice (DiGiovanna et al., 2016), it is possible that the lower power peaks around the stride and step frequencies may have reflected the cortical activity related to rhythmic walking movements.

A recent study examined gait-movement-related artifacts in EEG data by blocking the recording of electrophysiological signals (brain, eye, heart, and muscle activity) using a non-conductive layer (silicone swim cap) (Kline et al., 2015) and demonstrated that artifacts were smaller in electrodes in the central region (i.e., the vertex) compared with the peripheral regions, because movement artifacts were caused by vertical head acceleration. In the present study, widely distributed cortical activity, including that from central regions and peripheral regions (Figures 7A–7C), contributed to decoding.

We used a principal-component analysis (PCA)-based artifact rejection algorithm (ASR) to remove movement artifacts and other artifacts derived from muscle, heart, and eye activities. The ASR method removes high-variance artifact components from a dataset by comparison with a resting dataset (Mullen et al., 2015).

This method has been utilized in studies recording EEG signals during walking, and its effectiveness has been confirmed in several studies (Bulea et al., 2014; Nathan and Contreras-Vidal, 2016).

Taken together, the effects of movement artifacts on the current decoding results are not expected to be large. By using recently developed EEG cap hardware (dual electrode EEG cap), which can record EEG signals (cortical activity with artifact), and pure artifact signals, simultaneously (Nordin et al., 2018), we should be able to specifically evaluate the effect of artifacts on the decoding in the future.

Conclusions

We demonstrated that low-frequency cortical waves are informative for the decoding of muscle synergy activity during walking and that the decoding of individual muscle activity is based on muscle synergy-related cortical information. These results indicate cortical correlates of muscle synergy activation, possibly suggesting that the cortex is involved in hierarchical control of locomotor muscle activity through muscle synergies. These findings advance our understanding of relationships between brain activity and muscle synergies during walking. Moreover, they demonstrate the feasibility of neural decoding of muscle synergy activation, supporting its future contribution to the development of effective brain-muscle neuroprostheses to restore walking in patients with mobility limitations.

Limitations of the Study

Given that EEG signals are the summation of underlying cortical dynamics, there is a possibility that our results stemmed from the summation of cortical activity for the control of single muscles. However, a number of electrophysiological and anatomical studies have shown experimental evidence that the muscle representation in M1 is at the level of muscle synergy rather than a single muscle. For example, electrophysiological (Fetz and Cheney, 1980) and anatomical (Shinoda et al., 1981) studies have shown that individual corticospinal axons in monkeys branch widely in the spinal cord and innervate multiple motoneuron pools. In addition, it has been shown that microstimulation within M1 activates multiple muscles acting around more than one joint in cats (Armstrong and Drew, 1985) and monkeys (Overduin et al., 2012). The muscle-synergy-based representation in M1 was also reported in humans using transcranial magnetic stimulation (Gentner and Classen, 2006). Therefore our results may be based on the somatotopic feature in M1.

There are several limitations regarding muscle synergy extraction. The EMG normalization affects muscle synergy extraction. However, the decoding accuracy of muscle synergies was at a comparable level between those extracted from normalized (Figure 5) and non-normalized muscle synergies (Figure S3B). Therefore the normalization did not largely affect our decoding results. However, it should be kept in mind that the number of recorded muscles may affect the number of extracted muscle synergies by NMF (Steele et al., 2013; Zelik et al., 2014). Although the muscle synergies in this study were extracted from 13 leg muscles, the decoding of muscle synergies from a larger number of muscles would provide a more detailed understanding of modular strategies to simplify muscle control.

In this study we selected a slow walking speed (0.55 m/s) to minimize movement artifacts from the EEG based on previous EEG studies (Kline et al., 2015; Nathan and Contreras-Vidal, 2016). Nevertheless, it should be recognized that this walking speed is not ideal for examining muscle activity because EMG signals tend to be relatively small and noisy during slow-speed walking. For future studies, we should investigate the cortical involvement in the activation of muscle synergies during a more natural gait speed using EEG recoding systems that are less susceptible to the effects of movement artifacts and more sophisticated artifact removal techniques.

METHODS

All methods can be found in the accompanying Transparent Methods supplemental file.

SUPPLEMENTAL INFORMATION

Supplemental Information can be found online at https://doi.org/10.1016/j.isci.2019.04.008.

ACKNOWLEDGMENTS

This work was supported by a Grant-in-Aid for Japan Society for the Promotion of Science Fellows (JSPS, #18J01286) to H.Y., Grant-in-Aid for Scientific Research (A) from JSPS to K.N. (#18H00818), and the Core

Research for Evolutional Science and Technology (CREST) from Japan Science and Technology Agency (JST) to K.W. and K.N. (#JPMJCR14E4). We thank Dr. Ken Takiyama for helpful comments for the revision of our manuscript and Adonay Gebrehiwot for editing the English in the manuscript.

AUTHOR CONTRIBUTIONS

H.Y. and K.N. designed the experiment. H.Y. designed the current data analysis strategy. H.Y. and N. Kaneko collected data. H.Y. performed analyses. H.Y., T.O., and K.N. drafted the manuscript. All authors interpreted the data, discussed the findings, and approved the final version of the manuscript.

DECLARATION OF INTERESTS

The authors declare no competing interests.

Received: September 17, 2018
Revised: February 9, 2019
Accepted: April 4, 2019
Published: May 1, 2019

REFERENCES

Acharya, S., Fifer, M.S., Benz, H.L., Crone, N.E., and Thakor, N.V. (2010). Electrocorticographic amplitude predicts finger positions during slow grasping motions of the hand. J. Neural Eng. *7*, 046002.

Alibeji, N.A., Kirsch, N.A., and Sharma, N. (2015). A muscle synergy-inspired adaptive control scheme for a hybrid walking neuroprosthesis. Front. Bioeng. Biotech. *3*, 203.

Arad, E., Bartsch, R.P., Kantelhardt, J.W., and Plotnik, M. (2018). Performance-based approach for movement artifact removal from electroencephalographic data recorded during locomotion. PLoS One *13*, e0197153.

Armstrong, D., and Drew, T. (1984). Discharges of pyramidal tract and other motor cortical neurones during locomotion in the cat. J. Physiol. *346*, 471–495.

Armstrong, D., and Drew, T. (1985). Electromyographic responses evoked in muscles of the forelimb by intracortical stimulation in the cat. J. Physiol. *367*, 309–326.

Armstrong, D.M. (1988). The supraspinal control of mammalian locomotion. J. Physiol. *405*, 1–37.

Artoni, F., Fanciullacci, C., Bertolucci, F., Panarese, A., Makeig, S., Micera, S., and Chisari, C. (2017). Unidirectional brain to muscle connectivity reveals motor cortex control of leg muscles during stereotyped walking. Neuroimage *59*, 403–416.

Asanuma, H. (1975). Recent developments in the study of the columnar arrangement of neurons within the motor cortex. Physiol. Rev. *55*, 143–156.

Ball, T., Kern, M., Mutschler, I., Aertsen, A., and Schulze-Bonhage, A. (2009a). Signal quality of simultaneously recorded invasive and non-invasive EEG. Neuroimage *46*, 708–716.

Ball, T., Schulze-Bonhage, A., Aertsen, A., and Mehring, C. (2009b). Differential representation of arm movement direction in relation to cortical anatomy and function. J. Neural Eng. *6*, 016006.

Bouton, C.E., Shaikhouni, A., Annetta, N.V., Bockbrader, M.A., Friedenberg, D.A., Nielson, D.M., Sharma, G., Sederberg, P.B., Glenn, B.C., and Mysiw, W.J. (2016). Restoring cortical control of functional movement in a human with quadriplegia. Nature *533*, 247–250.

Bradberry, T.J., Gentili, R.J., and Contreras-Vidal, J.L. (2010). Reconstructing three-dimensional hand movements from noninvasive electroencephalographic signals. J. Neurosci. *30*, 3432–3437.

Bradford, J.C., Lukos, J.R., and Ferris, D.P. (2016). Electrocortical activity distinguishes between uphill and level walking in humans. J. Neurophysiol. *115*, 958–966.

Bruijn, S.M., Van Dieën, J.H., and Daffertshofer, A. (2015). Beta activity in the premotor cortex is increased during stabilized as compared to normal walking. Front. Hum. Neurosci. *9*, 593.

Bulea, T.C., Kim, J., Damiano, D.L., Stanley, C.J., and Park, H.-S. (2015). Prefrontal, posterior parietal and sensorimotor network activity underlying speed control during walking. Front. Hum. Neurosci. *9*, 247.

Bulea, T.C., Prasad, S., Kilicarslan, A., and Contreras-Vidal, J.L. (2014). Sitting and standing intention can be decoded from scalp EEG recorded prior to movement execution. Front. Neurosci. *8*, 376.

Cappellini, G., Ivanenko, Y.P., Poppele, R.E., and Lacquaniti, F. (2006). Motor patterns in human walking and running. J. Neurophysiol. *95*, 3426–3437.

Castermans, T., Duvinage, M., Cheron, G., and Dutoit, T. (2014). About the cortical origin of the low-delta and high-gamma rhythms observed in EEG signals during treadmill walking. Neurosci. Lett. *561*, 166–170.

Chao, Z.C., Nagasaka, Y., and Fujii, N. (2010). Long-term asynchronous decoding of arm motion using electrocorticographic signals in monkeys. Front. Neuroeng. *3*, 3.

Chvatal, S.A., and Ting, L.H. (2012). Voluntary and reactive recruitment of locomotor muscle synergies during perturbed walking. J. Neurosci. *32*, 12237–12250.

Clark, D.J., Ting, L.H., Zajac, F.E., Neptune, R.R., and Kautz, S.A. (2010). Merging of healthy motor modules predicts reduced locomotor performance and muscle coordination complexity post-stroke. J. Neurophysiol. *103*, 844–857.

Contreras-Vidal, J.L., Bortole, M., Zhu, F., Nathan, K., Venkatakrishnan, A., Francisco, G.E., Soto, R., and Pons, J.L. (2018). Neural decoding of robot-assisted gait during rehabilitation after stroke. Am. J. Phys. Med. Rehabil. *97*, 541–550.

d'Avella, A., and Bizzi, E. (2005). Shared and specific muscle synergies in natural motor behaviors. Proc. Natl. Acad. Sci. U S A *102*, 3076–3081.

d'Avella, A., Saltiel, P., and Bizzi, E. (2003). Combinations of muscle synergies in the construction of a natural motor behavior. Nat. Neurosci. *6*, 300–308.

Danner, S.M., Hofstoetter, U.S., Freundl, B., Binder, H., Mayr, W., Rattay, F., and Minassian, K. (2015). Human spinal locomotor control is based on flexibly organized burst generators. Brain *138*, 577–588.

DiGiovanna, J., Dominici, N., Friedli, L., Rigosa, J., Duis, S., Kreider, J., Beauparlant, J., Van Den Brand, R., Schieppati, M., and Micera, S. (2016). Engagement of the rat hindlimb motor cortex across natural locomotor behaviors. J. Neurosci. *36*, 10440–10455.

Dominici, N., Ivanenko, Y.P., Cappellini, G., d'Avella, A., Mondi, V., Cicchese, M., Fabiano, A., Silei, T., Di Paolo, A., Giannini, C., et al. (2011). Locomotor primitives in newborn babies and their development. Science *334*, 997–999.

Donati, A.R., Shokur, S., Morya, E., Campos, D.S., Moioli, R.C., Gitti, C.M., Augusto, P.B., Tripodi, S., Pires, C.G., and Pereira, G.A. (2016). Long-term training with a brain-machine interface-based gait protocol induces partial neurological

recovery in paraplegic patients. Sci. Rep. *6*, 30383.

Donoghue, J.P., and Wise, S.P. (1982). The motor cortex of the rat: cytoarchitecture and microstimulation mapping. J. Comp. Neurol. *212*, 76–88.

Drew, T., Kalaska, J., and Krouchev, N. (2008). Muscle synergies during locomotion in the cat: a model for motor cortex control. J. Physiol. *586*, 1239–1245.

Drew, T., and Marigold, D.S. (2015). Taking the next step: cortical contributions to the control of locomotion. Curr. Opini. Neurobiol. *33*, 25–33.

Duysens, J., Tax, A., Van der Doelen, B., Trippel, M., and Dietz, V. (1991). Selective activation of human soleus or gastrocnemius in reflex responses during walking and running. Exp. Brain Res. *87*, 193–204.

Everaert, D.G., Thompson, A.K., Chong, S.L., and Stein, R.B. (2010). Does functional electrical stimulation for foot drop strengthen corticospinal connections? Neurorehabil. Neural Repair *24*, 168–177.

Fetz, E.E., and Cheney, P.D. (1980). Postspike facilitation of forelimb muscle activity by primate corticomotoneuronal cells. J. Neurophysiol. *44*, 751–772.

Gentner, R., and Classen, J. (2006). Modular organization of finger movements by the human central nervous system. Neuron *52*, 731–742.

Giabbiconi, C.M., Dancer, C., Zopf, R., Gruber, T., and Müller, M.M. (2004). Selective spatial attention to left or right hand flutter sensation modulates the steady-state somatosensory evoked potential. Cogn. Brain Res. *20*, 58–66.

Gwin, J.T., Gramann, K., Makeig, S., and Ferris, D.P. (2011). Electrocortical activity is coupled to gait cycle phase during treadmill walking. Neuroimage *54*, 1289–1296.

Hall, T.M., de Carvalho, F., and Jackson, A. (2014). A common structure underlies low-frequency cortical dynamics in movement, sleep, and sedation. Neuron *83*, 1185–1199.

Hobson, J.A., and Pace-Schott, E.F. (2002). The cognitive neuroscience of sleep: neuronal systems, consciousness and learning. Nat. Rev. Neurosci. *3*, 679.

Ivanenko, Y.P., Poppele, R.E., and Lacquaniti, F. (2004). Five basic muscle activation patterns account for muscle activity during human locomotion. J. Physiol. *556*, 267–282.

Kim, A.W., Rosen, A.M., Brander, V.A., and Buchanan, T.S. (1995). Selective muscle activation following electrical stimulation of the collateral ligaments of the human knee joint. Arch. Phys. Med. Rehabil. *76*, 750–757.

King, C.E., Wang, P.T., McCrimmon, C.M., Chou, C.C., Do, A.H., and Nenadic, Z. (2015). The feasibility of a brain-computer interface functional electrical stimulation system for the restoration of overground walking after paraplegia. J. Neuroeng. Rehabil. *12*, 80.

Kline, J.E., Huang, H.J., Snyder, K.L., and Ferris, D.P. (2015). Isolating gait-related movement artifacts in electroencephalography during human walking. J. Neural Eng. *12*, 046022.

Kline, J.E., Huang, H.J., Snyder, K.L., and Ferris, D.P. (2016). Cortical spectral activity and connectivity during active and viewed arm and leg movement. Front. Neurosci. *10*, 91.

Kuo, A.D. (1999). Stabilization of lateral motion in passive dynamic walking. Int. J. Rob. Res. *18*, 917–930.

Kuroki, S., Yoshida, T., Tsutsui, H., Iwama, M., Ando, R., Michikawa, T., Miyawaki, A., Ohshima, T., and Itohara, S. (2018). Excitatory neuronal hubs configure multisensory integration of slow waves in association cortex. Cell Rep. *22*, 2873–2885.

La Fougere, C., Zwergal, A., Rominger, A., Förster, S., Fesl, G., Dieterich, M., Brandt, T., Strupp, M., Bartenstein, P., and Jahn, K. (2010). Real versus imagined locomotion: a [18 F]-FDG PET-fMRI comparison. Neuroimage *50*, 1589–1598.

Lebedev, M.A., and Nicolelis, M.A. (2006). Brain–machine interfaces: past, present and future. Trends Neurosci. *29*, 536–546.

Lebedev, M.A., and Nicolelis, M.A. (2017). Brain-machine interfaces: from basic science to neuroprostheses and neurorehabilitation. Physiol. Rev. *97*, 767–837.

Lee, D.D., and Seung, H.S. (1999). Learning the parts of objects by non-negative matrix factorization. Nature *401*, 788–791.

Maclellan, M., Ivanenko, Y., Massaad, F., Bruijn, S., Duysens, J., and Lacquaniti, F. (2014). Muscle activation patterns are bilaterally linked during split-belt treadmill walking in humans. J. Neurophysiol. *111*, 1541–1552.

Martino, G., Ivanenko, Y., Serrao, M., Ranavolo, A., Draicchio, F., Rinaldi, M., Casali, C., and Lacquaniti, F. (2018). Differential changes in the spinal segmental locomotor output in Hereditary Spastic Paraplegia. Clin. Neurophysiol. *129*, 516–525.

McCrea, D.A., and Rybak, I.A. (2008). Organization of mammalian locomotor rhythm and pattern generation. Brain Res. Rev. *57*, 134–146.

Miyai, I., Tanabe, H.C., Sase, I., Eda, H., Oda, I., Konishi, I., Tsunazawa, Y., Suzuki, T., Yanagida, T., and Kubota, K. (2001). Cortical mapping of gait in humans: a near-infrared spectroscopic topography study. Neuroimage *14*, 1186–1192.

Muceli, S., Boye, A.T., d'Avella, A., and Farina, D. (2010). Identifying representative synergy matrices for describing muscular activation patterns during multidirectional reaching in the horizontal plane. J. Neurophysiol. *103*, 1532–1542.

Mullen, T.R., Kothe, C.A., Chi, Y.M., Ojeda, A., Kerth, T., Makeig, S., Jung, T.-P., and Cauwenberghs, G. (2015). Real-time neuroimaging and cognitive monitoring using wearable dry EEG. IEEE Trans. Biomed. Eng. *62*, 2553–2567.

Nácher, V., Ledberg, A., Deco, G., and Romo, R. (2013). Coherent delta-band oscillations between cortical areas correlate with decision making. Proc. Natl. Acad. Sci. U S A *110*, 15085–15090.

Nakanishi, Y., Yanagisawa, T., Shin, D., Kambara, H., Yoshimura, N., Tanaka, M., Fukuma, R., Kishima, H., Hirata, M., and Koike, Y. (2017). Mapping ECoG channel contributions to trajectory and muscle activity prediction in human sensorimotor cortex. Sci. Rep. *7*, 45486.

Nathan, K., and Contreras-Vidal, J.L. (2016). Negligible motion artifacts in scalp electroencephalography (EEG) during treadmill walking. Front. Hum. Neurosci. *9*, 708.

Nicolelis, M.A. (2003). Brain–machine interfaces to restore motor function and probe neural circuits. Nat. Rev. Neurosci. *4*, 417–422.

Nordin, A.D., Hairston, W.D., and Ferris, D.P. (2018). Dual-electrode motion artifact cancellation for mobile electroencephalography. J. Neural Eng. *15*, 056024.

Overduin, S.A., d'Avella, A., Carmena, J.M., and Bizzi, E. (2012). Microstimulation activates a handful of muscle synergies. Neuron *76*, 1071–1077.

Patil, P.G., and Turner, D.A. (2008). The development of brain-machine interface neuroprosthetic devices. Neurotherapeutics *5*, 137–146.

Petersen, T.H., Willerslev-Olsen, M., Conway, B.A., and Nielsen, J.B. (2012). The motor cortex drives the muscles during walking in human subjects. J. Physiol. *590*, 2443–2452.

Presacco, A., Forrester, L.W., and Contreras-Vidal, J.L. (2012). Decoding intra-limb and inter-limb kinematics during treadmill walking from scalp electroencephalographic (EEG) signals. IEEE Trans. Neural Syst. Rehabil. Eng. *20*, 212–219.

Presacco, A., Goodman, R., Forrester, L., and Contreras-Vidal, J.L. (2011). Neural decoding of treadmill walking from noninvasive electroencephalographic signals. J. Neurophysiol. *106*, 1875–1887.

Rana, M., Yani, M.S., Asavasopon, S., Fisher, B.E., and Kutch, J.J. (2015). Brain connectivity associated with muscle synergies in humans. J. Neurosci. *35*, 14708–14716.

Rosenkranz, K., and Rothwell, J.C. (2004). The effect of sensory input and attention on the sensorimotor organization of the hand area of the human motor cortex. J. Physiol. *561*, 307–320.

Roy, F.D., and Gorassini, M.A. (2008). Peripheral sensory activation of cortical circuits in the leg motor cortex of man. J. Physiol. *586*, 4091–4105.

Saleh, M., Reimer, J., Penn, R., Ojakangas, C.L., and Hatsopoulos, N.G. (2010). Fast and slow oscillations in human primary motor cortex predict oncoming behaviorally relevant cues. Neuron *65*, 461–471.

Saltiel, P., d'Avella, A., Wyler-Duda, K., and Bizzi, E. (2015). Synergy temporal sequences and topography in the spinal cord: evidence for a traveling wave in frog locomotion. Brain Struct. Funct. *221*, 3869–3890.

Schabrun, S.M., Ridding, M.C., Galea, M.P., Hodges, P.W., and Chipchase, L.S. (2012). Primary sensory and motor cortex excitability are co-modulated in response to peripheral electrical nerve stimulation. PLoS One *7*, e51298.

Seeber, M., Scherer, R., Wagner, J., Solis-Escalante, T., and Müller-Putz, G.R. (2015). High and low gamma EEG oscillations in central sensorimotor areas are conversely modulated during the human gait cycle. Neuroimage *112*, 318–326.

Shinoda, Y., Yokota, J.-I., and Futami, T. (1981). Divergent projection of individual corticospinal axons to motoneurons of multiple muscles in the monkey. Neurosci. Lett. *23*, 7–12.

Srinivasan, R. (1999). Methods to improve the spatial resolution of EEG. Int. J. Bioelectromagn. *1*, 102–111.

Steele, K.M., Tresch, M.C., and Perreault, E.J. (2013). The number and choice of muscles impact the results of muscle synergy analyses. Front. Comput. Neurosci. *7*, 105.

Ting, L.H., Chiel, H.J., Trumbower, R.D., Allen, J.L., McKay, J.L., Hackney, M.E., and Kesar, T.M. (2015). Neuromechanical principles underlying movement modularity and their implications for rehabilitation. Neuron *86*, 38–54.

Tresch, M.C., Saltiel, P., and Bizzi, E. (1999). The construction of movement by the spinal cord. Nat. Neurosci. *2*, 162–167.

Van Der Meulen, M., Allali, G., Rieger, S.W., Assal, F., and Vuilleumier, P. (2014). The influence of individual motor imagery ability on cerebral recruitment during gait imagery. Hum. Brain Mapp. *35*, 455–470.

Veinante, P., and Deschênes, M. (2003). Single-cell study of motor cortex projections to the barrel field in rats. J. Comp. Neurol. *464*, 98–103.

Wagner, J., Solis-Escalante, T., Grieshofer, P., Neuper, C., Müller-Putz, G., and Scherer, R. (2012). Level of participation in robotic-assisted treadmill walking modulates midline sensorimotor EEG rhythms in able-bodied subjects. Neuroimage *63*, 1203–1211.

Waldert, S., Preissl, H., Demandt, E., Braun, C., Birbaumer, N., Aertsen, A., and Mehring, C. (2008). Hand movement direction decoded from MEG and EEG. J. Neurosci. *28*, 1000–1008.

Wang, C., Wai, Y., Kuo, B., Yeh, Y.-Y., and Wang, J. (2008). Cortical control of gait in healthy humans: an fMRI study. J. Neural Transm. (Vienna) *115*, 1149–1158.

Winter, D., and Yack, H. (1987). EMG profiles during normal human walking: stride-to-stride and inter-subject variability. Electroencephalogr. Clin. Neurophysiol. *67*, 402–411.

Witham, C.L., Wang, M., and Baker, S.N. (2007). Cells in somatosensory areas show synchrony with beta oscillations in monkey motor cortex. Eur. J. Neurosci. *26*, 2677–2686.

Yang, J.F., and Gorassini, M. (2006). Spinal and brain control of human walking: implications for retraining of walking. Neuroscientist *12*, 379–389.

Yokoyama, H., Ogawa, T., Kawashima, N., Shinya, M., and Nakazawa, K. (2016). Distinct sets of locomotor modules control the speed and modes of human locomotion. Sci. Rep. *6*, 36275.

Yokoyama, H., Ogawa, T., Shinya, M., Kawashima, N., and Nakazawa, K. (2017). Speed dependency in α-motoneuron activity and locomotor modules in human locomotion: indirect evidence for phylogenetically conserved spinal circuits. Proc. Biol. Sci. *284*, 20170290.

Zelik, K.E., La Scaleia, V., Ivanenko, Y.P., and Lacquaniti, F. (2014). Can modular strategies simplify neural control of multidirectional human locomotion? J. Neurophysiol. *111*, 1686–1702.

ISCI, Volume *15*

Supplemental Information

Cortical Correlates of Locomotor Muscle Synergy Activation in Humans: An Electroencephalographic Decoding Study

Hikaru Yokoyama, Naotsugu Kaneko, Tetsuya Ogawa, Noritaka Kawashima, Katsumi Watanabe, and Kimitaka Nakazawa

Supplemental Information

Supplemental Figures

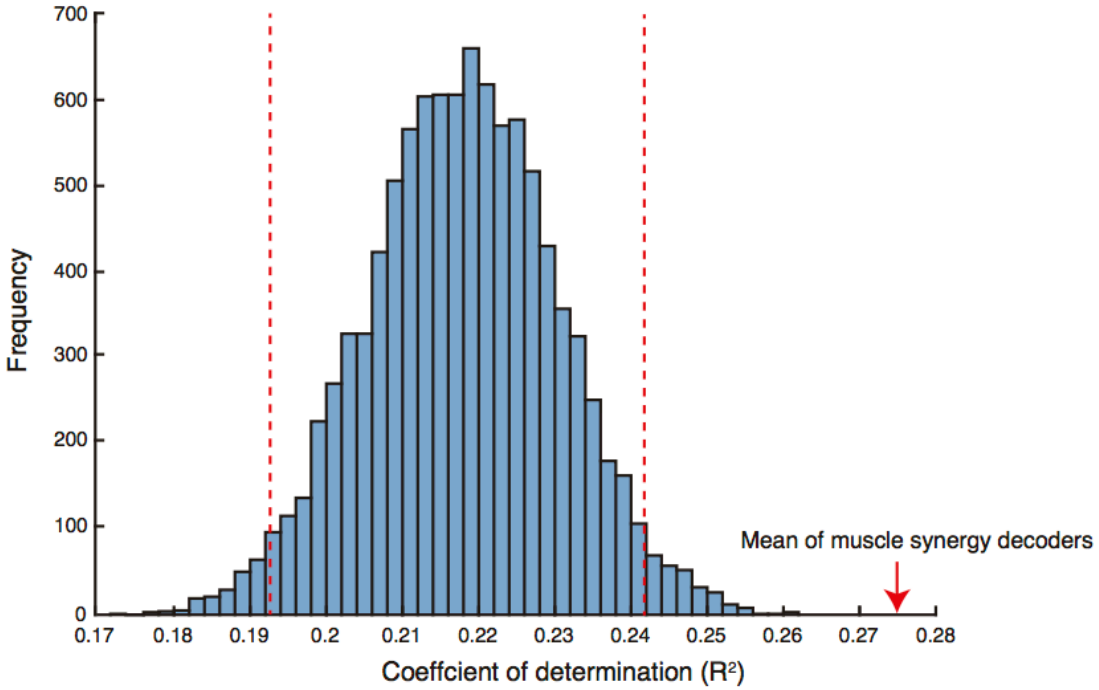

Figure S1. Histogram of the distribution of the across-participant mean of the overall decoding accuracy of individual muscle decoders from the same number of randomly selected muscles as the muscle synergies. Related to Figure 5. Vertical red lines indicate the 95% confidence intervals. The red arrow indicates the across-participant mean of the overall decoding accuracy of muscle synergy decoders.

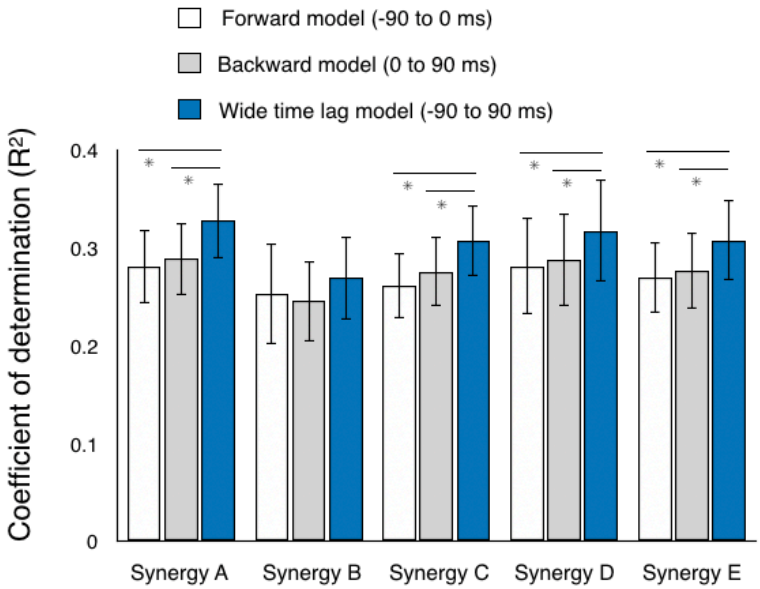

Figure S2. Decoding accuracy (coefficient of determination) of muscle synergy decoders in three different decoder types (Forward, Backward and Wide time lag models). Related to Figure 5. The mean and SEM across all participants are shown. Asterisks indicate significant differences (*: $p < 0.05$, FDR corrected for multiple comparisons; see Table S7 for detailed statistical values).

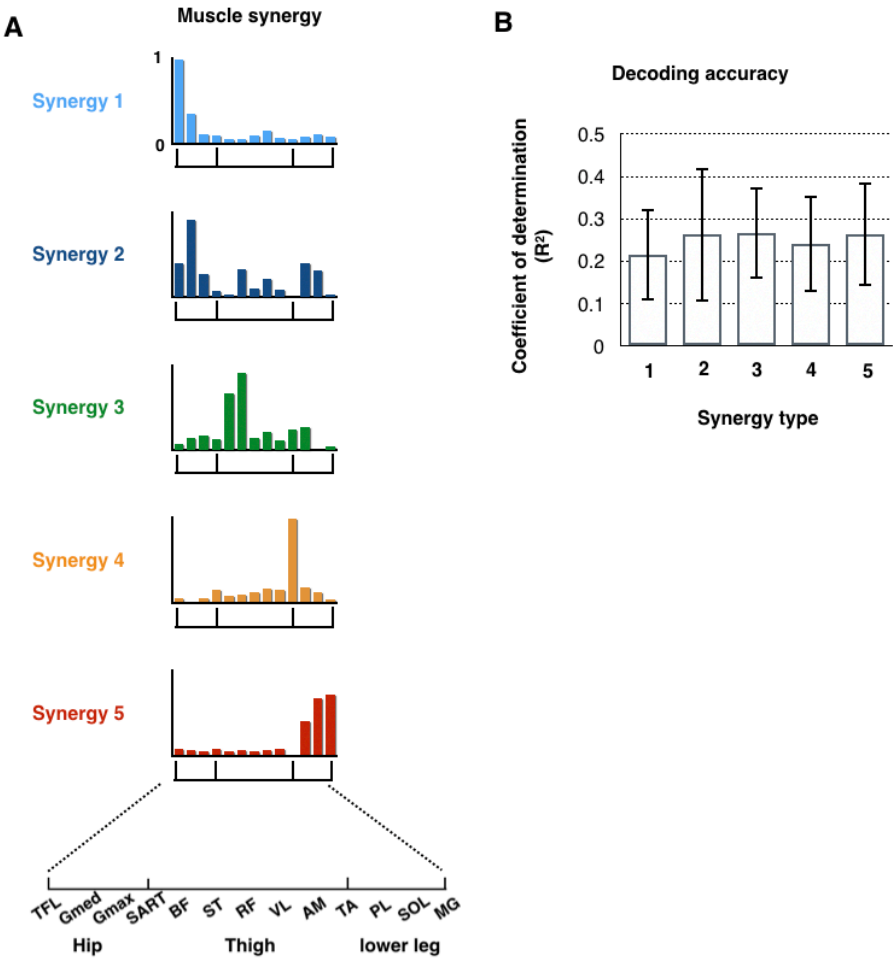

Figure S3. Five extracted types of locomotor muscle synergies from non-normalized muscle activity (A) and decoding accuracy for the muscle synergies (B). Related to Figure 5. (A) Averaged muscle synergies (bars, spatial muscle weightings) across participants in each type are shown. Each bar height represents the relative level of activation of each muscle synergy. An enlarged view of the x-axis is shown at the bottom. (B) The mean and SD of the decoding accuracy (coefficient of determination) across participants for each muscle synergy type are shown.

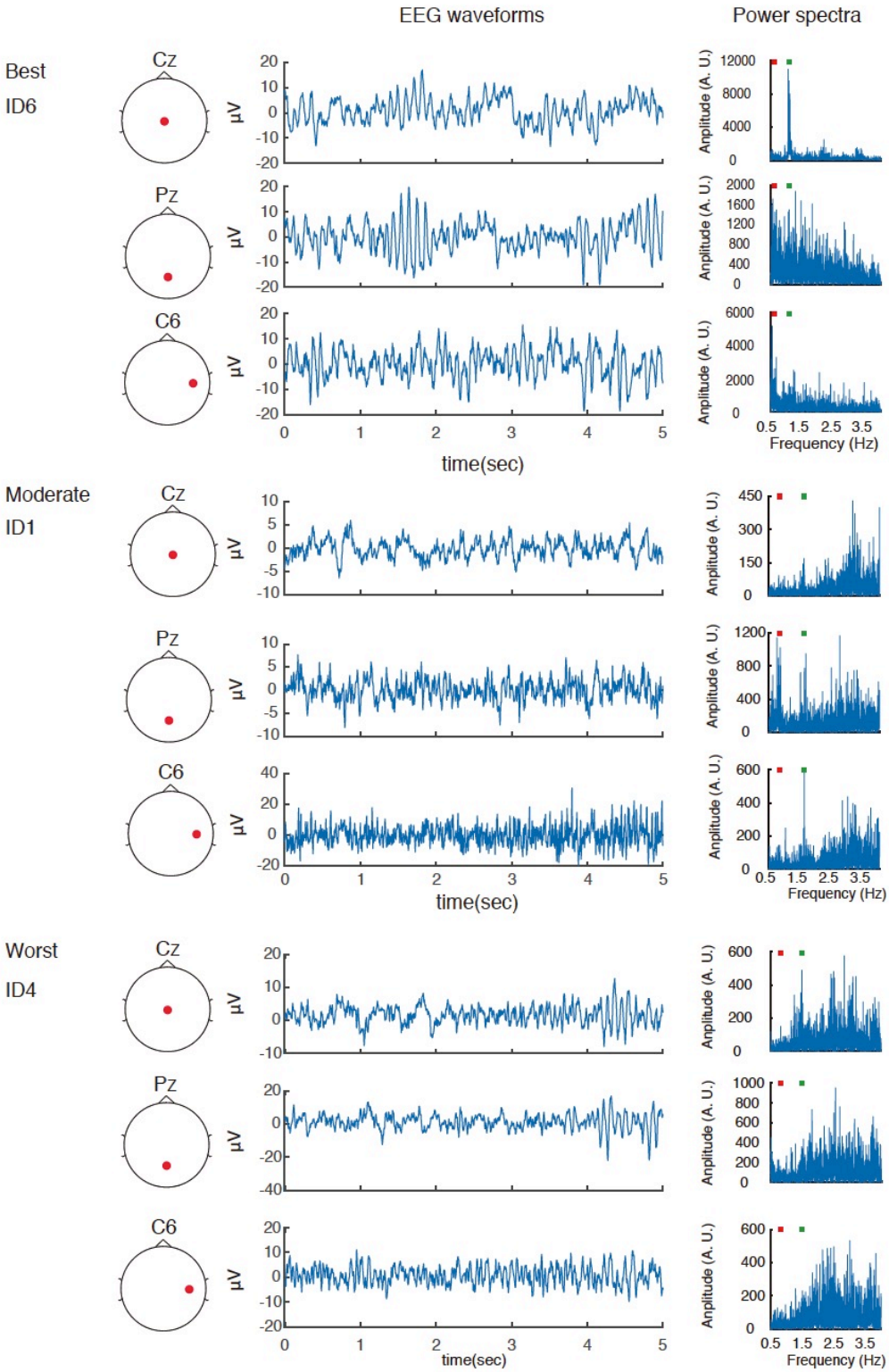

Figure S4. Examples of EEG data from three electrodes (Cz, Pz, C6), for the diversity of their spatial localizations (top, back, and right side of the head, respectively), from participants who showed the best, moderate, and worst decoding accuracies, respectively. Related to Figure 5 and Figure7. The central column shows 5 seconds of EEG signals after artifact subspace reconstruction (ASR) just before low-pass filtering (4 Hz) to obtain slow cortical potentials. The

right column shows the power spectra of the electrodes in the delta band (0.5–4 Hz). Red and green squares indicate their stride and step frequency, respectively.

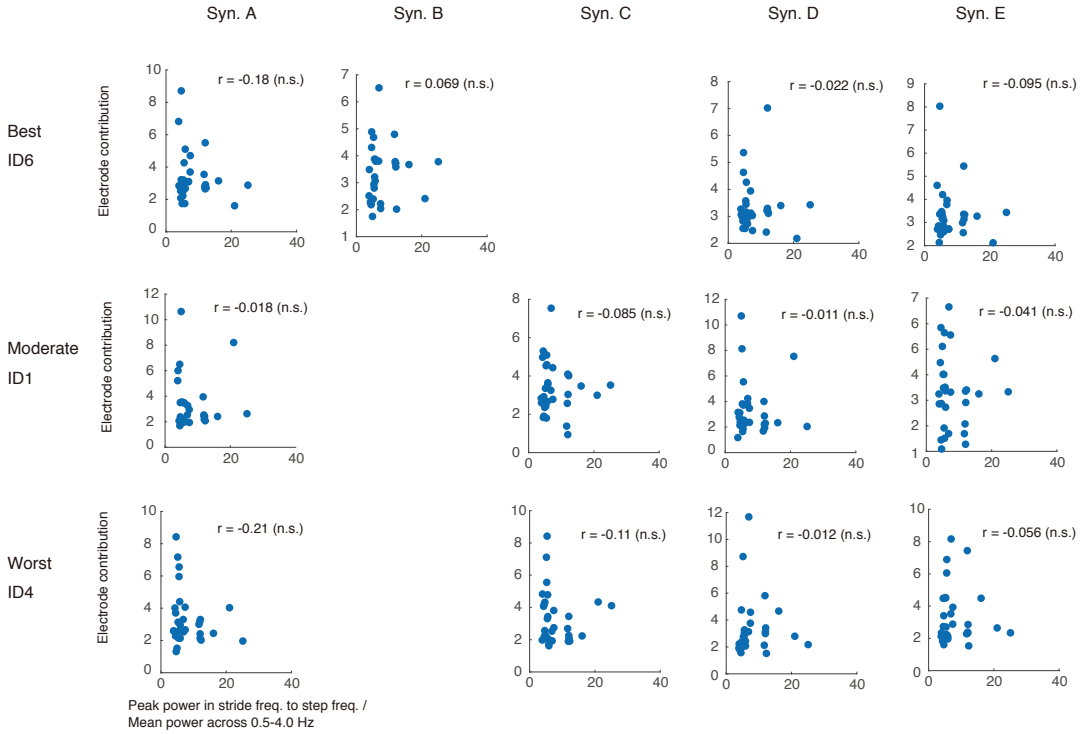

Figure S5. Relation between electrode contribution to the decoding and movement artifact size of participants who showed the best, moderate and worst decoding accuracy. Related to Figure 5 and Figure7. Each plot indicate each electrode data. Correlation coefficients are shown.

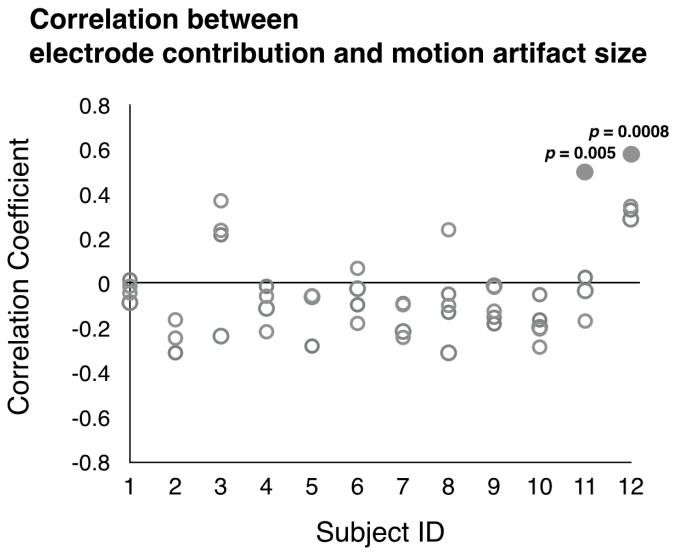

Figure S6. Correlation between electrode contribution to the decoding and movement artifact size for all muscle synergy decoders in all participants. Related to Figure 5 and Figure7. Each plot indicates the correlation value for each muscle synergy decoder. Open and filled circles indicate statistically non-significant and significant correlation values, respectively.

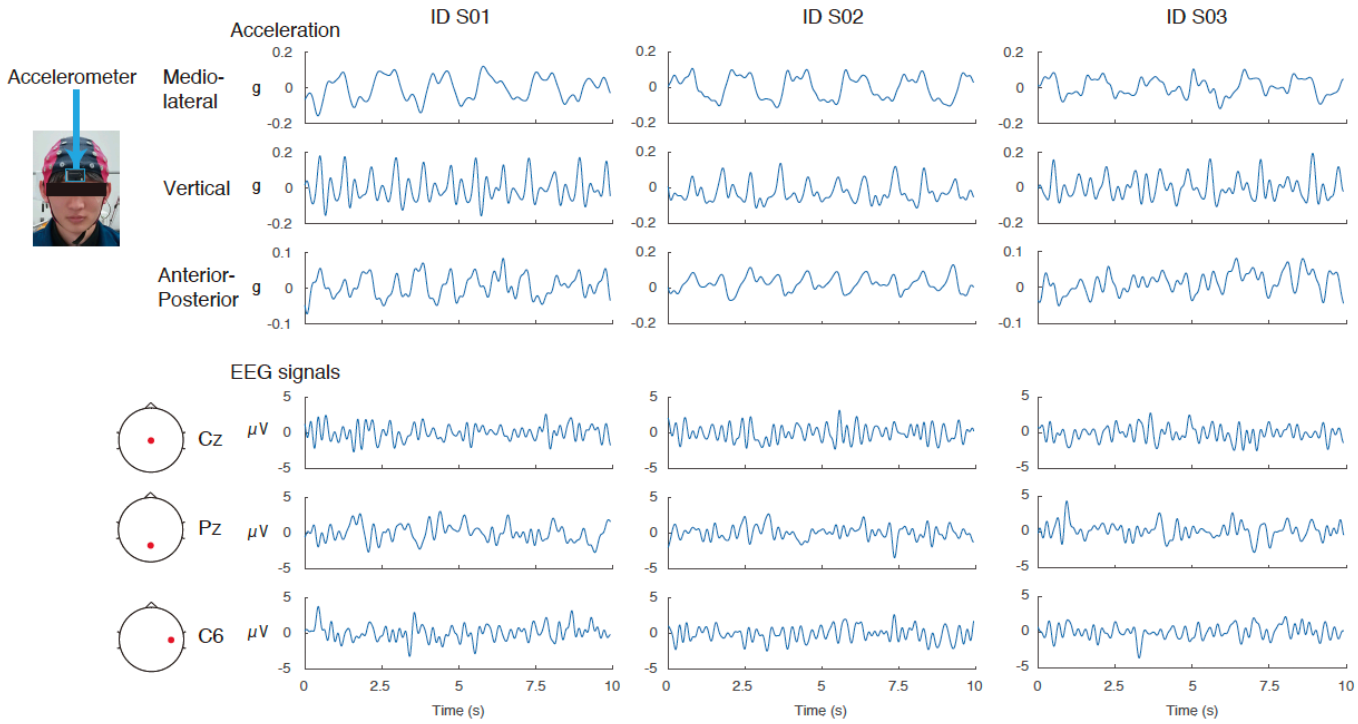

Figure S7. Time courses of head accelerations (mediolateral, vertical, and anterior-posterior), and EEG signals (slow cortical potentials) from three electrodes (Cz, Pz, C6), for the diversity of their spatial localizations (top, back, and right side of the head, respectively), from all three participants in the supplemental experiment. Related to Figure 5 and Figure7.

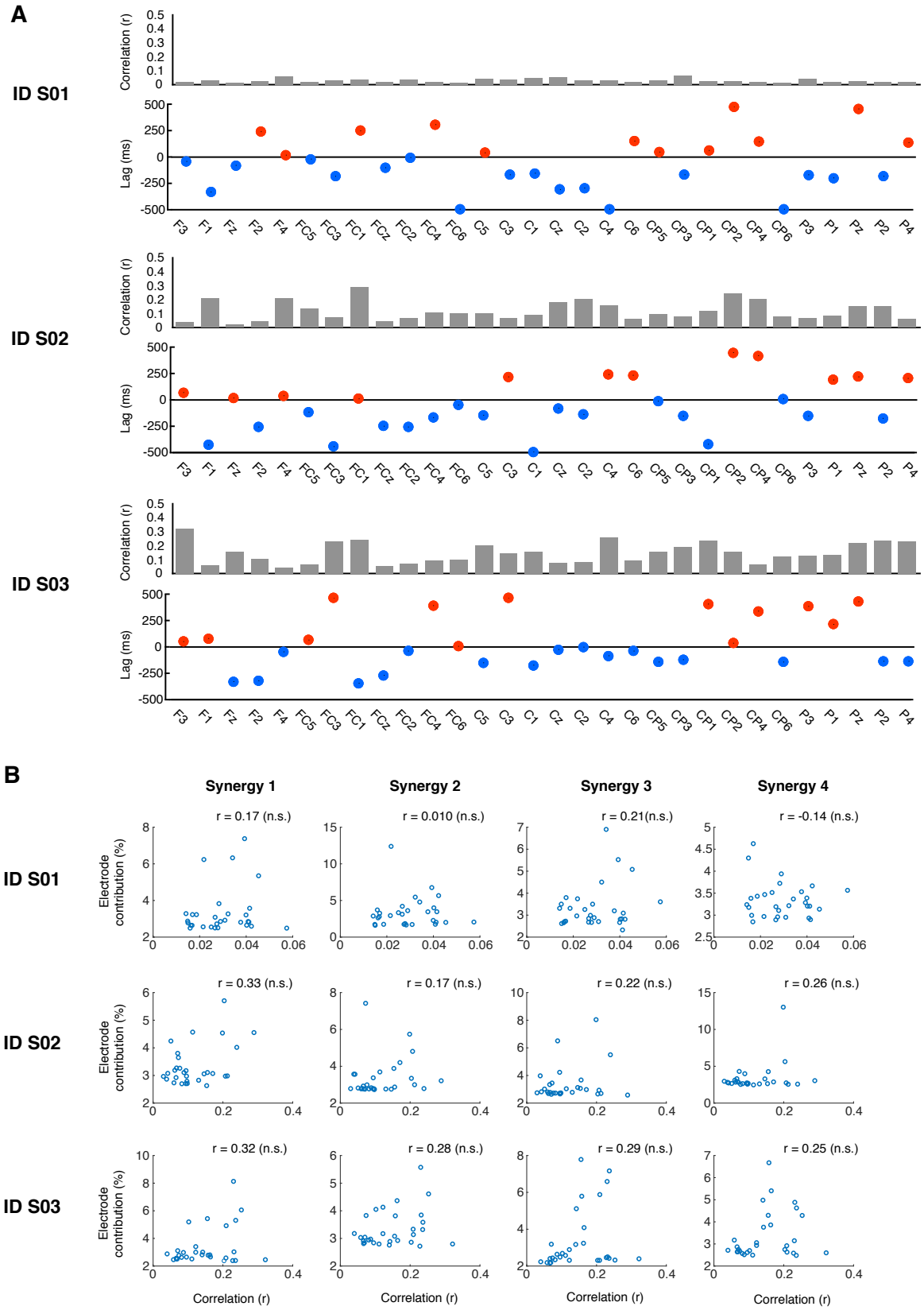

Figure S8. Cross-correlation results between vertical head accelerations and slow cortical potentials. Related to Figure 5 and Figure7. (A) Peak correlation coefficient values are shown in the bar graphs. Time lags at the peak correlation values are shown in the plot graphs. Red plots indicate that EEG signals are preceding the head accelerations; blue plots indicate that head accelerations are preceding the EEG signals. (B) Relation between the peak correlation values of the cross-correlation analysis and electrode contribution in all electrodes in each muscle synergy decoder.

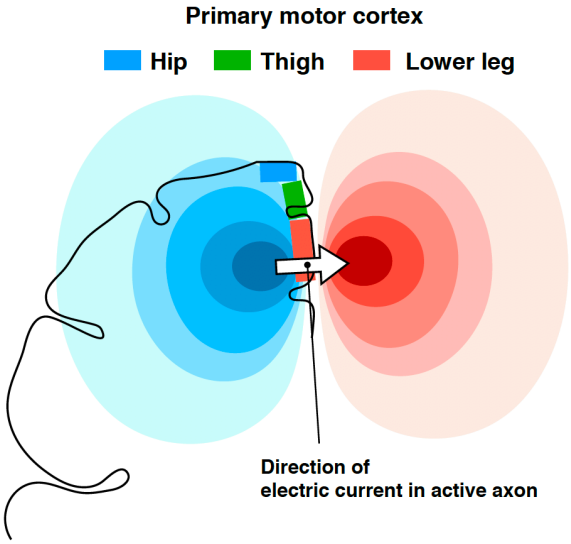

Figure S9. Schematic illustration of the electrical source in the left primary motor cortex corresponding to the right lower leg muscle area and the resulting electrical field in the brain. Related to Figure7. Blue, green, and red rectangles represent the cortical areas corresponding to the hip, thigh, and lower leg muscles, respectively. The white arrow indicates direction of electric current of an electric source (i.e., neural column). Darker areas of color indicate a stronger electric field. Red and blue areas indicate positive and negative values, respectively.

Supplemental tables

Table S1. Characteristics of each type of locomotor muscle synergy. Related to Figure 3.

Type	Activation timing	Major muscles
Synergy A	Mid stance phase	TFL, Gmed, and GM
Synergy B	Mid swing phase and early stance phase	ST, RF, VL, AM, and TA
Synergy C	Last swing to initial stance phase	BF, ST
Synergy D	Mid swing phase and transition from the stance phase to the swing phase	AM, TA
Synergy E	Latter half of stance phase	SOL and MG

Table S2. Summary of statistical analyses for comparisons of decoding accuracy among each ROI and all electrodes for Synergy A. Related to Figure 7.

Method	Pair	Value
ANOVA		$F_{4,48} = 19.15$, $p = 1.8\times10^{-9}$
Multiple t-test with FDR correction	Frontal vs. Cental	p = 0.50
Multiple t-test with FDR correction	Frontal vs. Lateral	p = 0.33
Multiple t-test with FDR correction	Frontal vs. Parietal	p = 0.29
Multiple t-test with FDR correction	Frontal vs. All	p = 0.00010
Multiple t-test with FDR correction	Central vs. Lateral	p = 0.16
Multiple t-test with FDR correction	Central vs. Parietal	p = 0.13
Multiple t-test with FDR correction	Central vs. All	p = 6.3e-05
Multiple t-test with FDR correction	Lateral vs. Parietal	p = 0.52
Multiple t-test with FDR correction	Lateral vs. All	p = 7.1e-05
Multiple t-test with FDR correction	Parietal vs. All	p = 0.00010

Table S3. Summary of statistical analyses for comparisons of decoding accuracy among each ROI and all electrodes for Synergy B. Related to Figure 7.

Method	Pair	Value
ANOVA		$F_{4,20} = 11.32$, $p = 5.8\times10^{-5}$
Multiple t-test with FDR correction	Frontal vs. Cental	p = 0.16
Multiple t-test with FDR correction	Frontal vs. Lateral	p = 0.74
Multiple t-test with FDR correction	Frontal vs. Parietal	p = 0.74
Multiple t-test with FDR correction	Frontal vs. All	p = 0.027
Multiple t-test with FDR correction	Central vs. Lateral	p = 0.16
Multiple t-test with FDR correction	Central vs. Parietal	p = 0.46
Multiple t-test with FDR correction	Central vs. All	p = 0.027
Multiple t-test with FDR correction	Lateral vs. Parietal	p =0.47
Multiple t-test with FDR correction	Lateral vs. All	p = 0.027
Multiple t-test with FDR correction	Parietal vs. All	p = 0.036

Table S4. Summary of statistical analyses for comparisons of decoding accuracy among each ROI and all electrodes for Synergy C. Related to Figure 7.

Method	Pair	Value
ANOVA		$F_{4,36} = 17.57$, $p = 4.4\times10^{-8}$
Multiple t-test with FDR correction	Frontal vs. Cental	p = 0.80
Multiple t-test with FDR correction	Frontal vs. Lateral	p = 0.45
Multiple t-test with FDR correction	Frontal vs. Parietal	p = 0.77
Multiple t-test with FDR correction	Frontal vs. All	p = 0.0013
Multiple t-test with FDR correction	Central vs. Lateral	p = 0.77
Multiple t-test with FDR correction	Central vs. Parietal	p = 0.77
Multiple t-test with FDR correction	Central vs. All	p = 0.00026
Multiple t-test with FDR correction	Lateral vs. Parietal	p = 0.99
Multiple t-test with FDR correction	Lateral vs. All	p = 0.00023
Multiple t-test with FDR correction	Parietal vs. All	p = 0.00023

Table S5. Summary of statistical analyses for comparisons of decoding accuracy among each ROI and all electrodes for Synergy D. Related to Figure 7.

Method	Pair	Value
ANOVA		$F_{4,24} = 9.18$, $p = 0.00012$
Multiple t-test with FDR correction	Frontal vs. Cental	p = 0.28
Multiple t-test with FDR correction	Frontal vs. Lateral	p = 0.93
Multiple t-test with FDR correction	Frontal vs. Parietal	p = 0.82
Multiple t-test with FDR correction	Frontal vs. All	p = 0.0069
Multiple t-test with FDR correction	Central vs. Lateral	p = 0.30
Multiple t-test with FDR correction	Central vs. Parietal	p = 0.68
Multiple t-test with FDR correction	Central vs. All	p = 0.0074
Multiple t-test with FDR correction	Lateral vs. Parietal	p = 0.82
Multiple t-test with FDR correction	Lateral vs. All	p = 0.0069
Multiple t-test with FDR correction	Parietal vs. All	p = 0.0069

Table S6. Summary of statistical analyses for comparisons of decoding accuracy among each ROI and all electrodes for Synergy E. Related to Figure 7.

Method	Pair	Value
ANOVA		$F_{4,52} = 16.11$, $p = 1.22\times10^{-8}$
Multiple t-test with FDR correction	Frontal vs. Cental	p = 0.023
Multiple t-test with FDR correction	Frontal vs. Lateral	p = 0.57
Multiple t-test with FDR correction	Frontal vs. Parietal	p = 0.30
Multiple t-test with FDR correction	Frontal vs. All	p = 0.00033
Multiple t-test with FDR correction	Central vs. Lateral	p = 0.053
Multiple t-test with FDR correction	Central vs. Parietal	p = 0.0082
Multiple t-test with FDR correction	Central vs. All	p = 0.0013
Multiple t-test with FDR correction	Lateral vs. Parietal	p = 0.84
Multiple t-test with FDR correction	Lateral vs. All	p = 0.0012
Multiple t-test with FDR correction	Parietal vs. All	p = 0.00040

Table S7. Summary of statistical analyses for comparisons of decoding accuracy between three types of decoders (Forward, Backward and Wide time lag decoders). Related to Figure 5. See also Figure S2.

Method	Statistical value				
	Synergy A	Synergy B	Synergy C	Synergy D	Synergy E
ANOVA	$F_{2,24} = 19.08$, $p = 1.1\times10^{-5}$	$F_{2,10} = 2.15$, $p = 0.168$	$F_{2,18} = 32.99$, $p = 9.6\times10^{-7}$	$F_{2,12} = 16.87$, $p = 0.00033$	$F_{2,26} = 14.35$, $p = 6.3\times10^{-5}$
Multiple t-test with FDR correction (Forward vs. Backward)	p = 0.6803	-	p = 0.054	p = 0.65	p = 0.71
Multiple t-test with FDR correction (Forward vs. Wide time lag)	p = 9.1e-06	-	p = 0.00015	p = 0.0060	p = 0.0030
Multiple t-test with FDR correction (Backward vs. Wide time lag)	p = 0.0056	-	p = 0.0013	p = 0.012	p = 0.00045

Table S8. Summary of decoding accuracy in the supplemental experiment. Related to Figure 5 and Figure 7. See also Figure S7 and Figure S8.

	ID-S01	ID-S02	ID-S03	All muscle synergies from three participants
R^2 (Mean (SD))	0.29 (0.038)	0.21 (0.035)	0.20 (0.062)	0.23 (0.060)

Transparent Methods

Experimental model and subject details

Participants

In this study, we conducted two experiments: 1) the main experiment and 2) the supplemental experiment. Twelve healthy male volunteers (age, 23–31 years) participated in the main experiment. Additionally, three healthy male volunteers (age, 24–28 years) participated in the supplemental experiment. Each participant provided written informed consent. The experiments were performed in accordance with the Declaration of Helsinki and with the approval of the Ethics Committee of the Graduate School of Arts and Sciences, University of Tokyo.

Method details

Main experiment

Experimental design and setup

Participants walked on a treadmill (Bertec, Columbus, OH, USA) at 0.55 m/s for 7 min 30 seconds. The last seven minutes of data were used for the analysis. The slow walking speed was chosen based on two previous studies examining the effects of walking speed on movement artifacts in EEG signals (Kline et al., 2015; Nathan and Contreras-Vidal, 2016): Kline et al. (2015) used an experimental method to isolate and record independent movement artifacts with a silicone swim cap (nonconductive material), and reported large movement artifacts at walking speeds faster than 0.8 m/s. A study that analyzed relationships between head acceleration and motion artifacts in EEG signals indicated that recordings were robust at gait speeds below 3.0 km/h (0.83 m/s) (Nathan and Contreras-Vidal, 2016). As a static baseline condition, the participants sat on a chair for two minutes.

Data collection

Three-dimensional ground reaction forces (GRF) were recorded from force plates under the right and left belts of the treadmill (sampling rate: 1000 Hz). GRF data were smoothed with a low-pass filter (zero-lag Butterworth filter, 5 Hz cutoff). MATLAB 2016b (MathWorks, Natick, MA, USA) was used to perform all the post-processing analyses offline.

Surface electromyographic (EMG) signals were recorded from the following 13 leg muscles on the right side using a wireless EMG system (Trigno Wireless System, DelSys Inc., Boston, MA, USA): tensor fasciae latae (TFL), gluteus maximus (GM), gluteus medius (Gmed), sartorius (SART), biceps femoris (BF), semitendinosus (ST), rectus femoris (RF), vastus lateralis (VL), adductor magnus (AM), tibialis anterior (TA), peroneus longus (PL), soleus (SOL), and gastrocnemius medialis (MG). EMGs were amplified (with 300 gain preamplifier), band-pass filtered (20–450 Hz), and sampled at 1000 Hz.

A 64-channel EEG cap (Waveguard original, ANT Neuro b.v., Enschede, Netherlands) and a mobile EEG amplifier (eego sports, ANT Neuro b.v., Enschede, Netherlands) were used to record EEG signals at a sampling frequency of 500 Hz. Arrangement of the electrodes was according to the international 10–20 electrode system. EEG signals were referenced to CPz and a ground electrode was placed on AFz. Electrode impedances were kept below 30 kΩ (10 kΩ in most electrodes), which was substantially below the recommended impedance (below 50 kΩ) for the high-impedance EEG amplifier. Peripheral channels, which are prone to contamination by facial/cranial muscle activity and eye blinks, were removed from the offline analysis (channels labeled Fp, AF, FT, T, TP, O, PO, and F5-8, P5-8) (Bulea et al., 2014), resulting in the 30 channels presented in Figure 1.

EMG processing and extraction of locomotor muscle synergies

Figure 2 shows an overview of our decoding methodology. From the recorded EMG signals, EMG envelopes and muscle synergies were used for the neural decoding analysis.

First, the recorded EMG data were high-pass filtered (zero-lag fourth-order Butterworth at 30 Hz), demeaned, full-wave rectified, and smoothed with a low-pass filter (zero-lag fourth-order Butterworth at 4 Hz cutoff) to obtain EMG envelopes (Clark et al., 2010). EMG envelopes were resampled at 100 Hz. The amplitude of EMG envelopes for each muscle was normalized to the maximum value for that muscle during the walking task. Muscle synergies were extracted from the processed EMG envelopes using non-negative matrix factorization (NMF) (Clark et al., 2010; d'Avella and Bizzi, 2005; Dominici et al., 2011; Lee and Seung, 1999; Yokoyama et al., 2016). For each participant, muscle synergies were extracted from the EMG dataset organized as a matrix with 13 muscles × 42000 variables (i.e., 100 Hz × 420 sec [7 min]). Using NMF, the EMG matrix (*M*) was decomposed into spatial muscle weightings (*S*), which correspond to the muscle synergies and their temporal activations (*C*) according to formula (1):

$$M = S \cdot C + E \quad (1)$$

where *M* (*m* × *t* matrix, where *m* is the number of muscles and *t* is the number of samples in the EMG data matrix) is a linear combination of muscle synergies, *S* (*m* × $N_{synergy}$ matrix, where $N_{synergy}$ is the number of muscle synergies), and their temporal activation patterns, *C* ($N_{synergy}$ × *t* matrix), and *E* is the residual error matrix. The number of muscle synergies, $N_{synergy}$, was determined by iterating each possible $N_{synergy}$ from 1 to 10. For each $N_{synergy}$, the goodness of fit was evaluated based on the variance accounted for (VAF) (Torres-Oviedo et al., 2006). Based on the VAF, the optimal $N_{synergy}$ was defined as the minimum value fulfilling two criteria: (1) the number of muscle synergies achieving VAF > 90% (Torres-Oviedo et al., 2006), and (2) the number to which adding an additional muscle synergy did not increase VAF by > 5% (Frere and Hug, 2012). Then,

we clustered the extracted muscle synergies using hierarchical clustering analysis to examine the extracted types of muscle synergies (Ward's method, correlation distance) based on muscle weightings, as in our previous studies (Yokoyama et al., 2017a; Yokoyama et al., 2016; Yokoyama et al., 2017b). The gap statistic method was used to define the optimal number of clusters (Tibshirani et al., 2001).

EEG pre-processing

In the current study, fluctuations in the amplitude of slow cortical potentials (0.5 – 4 Hz in the time domain) were used for the neural decoding analysis (Figure 2) based on a similar methodology used in previous studies (Bradberry et al., 2010; Contreras-Vidal et al., 2018; Nakanishi et al., 2017; Presacco et al., 2012; Presacco et al., 2011). EEG data analysis was performed using custom programs in MATLAB incorporating functions of EEGLAB 14.1b (Delorme and Makeig, 2004). The EEG signals were band-pass filtered between 0.5−100 Hz with a Butterworth filter (fourth-order). The "cleanline" function in EEGLAB was used to remove power line noise (50 Hz). Next, the EEG signals were resampled at 100 Hz. Then, we checked noisy EEG channels based on two criteria adopted from a previous study (Gwin et al., 2011): 1) standard deviation greater than 1000 μV, and 2) kurtosis of more than five standard deviations from the mean. In this study, no EEG electrode satisfied the criteria in all the participants. Since various types of artifacts were potentially introduced in the EEG data, we used an artifact rejection method called Artifact Subspace Reconstruction (ASR) (Mullen et al., 2015) in EEGLAB to remove artifacts derived from walking, eye blinks, muscle, and heart activity. Next, the cleaned EEG signals were low-pass filtered at 4 Hz with a zero-phase Butterworth filter (fourth-order) and re-referenced to a common average reference. Finally, the amplitude of each electrode was normalized by calculating the standard z-score.

Neural decoding of muscle synergy and individual muscle activation

To continuously decode the activation of muscle synergies and individual muscles from the slow cortical potentials, we designed a time-embedded (10 lags, corresponding to 0 ms to -90 ms) linear decoding model, called the Wiener filter (Bradberry et al., 2010; Carmena et al., 2003; Presacco et al., 2011), for the muscle synergy and EMG envelope data. The linear model is given by:

$$y(t) = b + \sum_{i=1}^{N_{electrode}} \sum_{j=1}^{L} W_{ij} \cdot x_i[t-(j-1)] + e(t) \quad (2)$$

where $y(t)$ is the predicted time series activation of each muscle synergy or EMG envelope at time t, b is the intercept, $N_{electrode}$ (= 30) is the number of electrodes, L (=10) is the number of time lags, $x(t)$ is the normalized slow cortical potentials at electrode i at time t, W_{ij} is the weights at electrode i and time lag j, and $e(t)$ is the residual error. The time lag was selected to use the cortical information ahead of the muscle activity because we were interested in examining the cortical descending control of muscle activity. The maximum time lag (-90 ms) was chosen based on the traveling time of the cortical command to the muscles examined by TMS (~35−40 ms) (Nielsen et al., 1995; Terao et al., 2000). Thus, we set the time lag to sufficiently contain the traveling time. The parameters of the model were calculated with multidimensional generalized linear regression (Bradberry et al., 2010; Carmena et al., 2003; Presacco et al., 2011) using the "glm" function in MATLAB (Gaussian distribution condition). Neural decoders were designed separately for each participant and each decoded parameter (i.e., each muscle synergy and each EMG envelope).

In addition to the above-explained forward decoder (-90 to 0 ms, forward model), we performed decoding analyses of muscle synergy activation using two additional types of decoders, which used positively time-lagged information (0 to 90 ms, backward model) and widely time-lagged information (-90 to 90 ms, wide time lag model).

For assessing the predictive accuracy of each decoder, a seven-fold cross-validation procedure was performed. Thus, the data recorded during the 7 min walking task were divided into 7 segments (1 min each). Six segments were used for training data while the remaining segment was used for testing the decoding model. In the cross-validation, the temporal activation patterns of muscle synergies (C in equation (1)) for the test data were calculated using the NMF algorithm initialized with the spatial weightings of muscle synergies (S in equation (1)) extracted from the training data and updating only the temporal activation patterns of the synergies to reconstruct the muscle activation patterns of test data (Berger et al., 2013; Clark et al., 2010; d'Avella et al., 2006; Yokoyama et al., 2016). The EEG signals for the test data were normalized by subtracting a mean value from the training data and then dividing by the standard deviation of the training data. This procedure was repeated for all possible combinations (i.e., seven times). Coefficient of determination (R^2) were calculated between the real activation and the decoded activation at each decoder in each iteration. To compare the overall decoding accuracy between the two types of decoders (muscle synergy decoders vs. individual muscle decoders), overall R^2 values were calculated for each type per participant. To minimize the effects of skewness in the sampling distributions on the correlation coefficients, each coefficient of determination value was averaged after Fisher's Z-transformation (Corey et al., 1998). After averaging, the Z-values were back-transformed to the scale of Pearson's r values.

The difference in the number of decoders (individual muscles: 13, muscle synergies: 3−5 depending on participants) may have possibly affected the comparisons of the overall decoding accuracy, as the sample mean of the larger sample size more accurately estimates the population mean. To overcome this issue, the overall decoding accuracy was calculated using the same number of randomly sampled individual muscle decoders with muscle synergies from 13 muscles per participants (sampling without replacement). In this analysis, the Z-transformed decoding accuracy values were randomly sampled and averaged. We then calculated the across-participant mean of the overall decoding accuracy for individual muscle decoders. The procedure was iterated 10000 times, and we calculated the 95% confidence interval of the distribution of the 10000 values of the across-participant mean of the overall decoding accuracy of individual muscles. Then, we tested whether the across-participant mean of the overall decoding accuracy for muscle synergy decoders was larger than the 95% confidence interval.

Chance levels of neural decoding were evaluated by randomizing the EEG phase (Theiler et al., 1992). Phase-randomized EEG signals were generated using the fast Fourier transform of a time series throughout the recording duration to randomize the phase in the Fourier domain while keeping the power spectrum unchanged; then the inverse Fourier transform was performed to back to the time domain. After phase-randomization, the power spectrum was preserved in the surrogate data, but the phase relation to the muscle activity was disrupted. When decoding from the time-domain EEG signals, it is assumed that the signals are phase-locked to muscle activity and that a randomization of the phase can provide a chance level of the decoding accuracy. The same decoding procedure was performed using the phase-randomized EEG signals. We generated 100 phase-randomized EEG datasets for each participant

and performed neural decoding using each randomized dataset to obtain confidence intervals for the decoding accuracy.

Analysis of relationships between muscle synergy decoders and individual muscle decoders

We reconstructed individual muscle activations by summing the outputs of each decoded muscle synergy to test whether the variability in decoding accuracy in individual muscles would be reproduced by individual muscle activations indirectly decoded from muscle synergy activations decoded from muscle synergy decoders. The output of a decoded muscle synergy was explained by the product of the muscle weighting component and the decoded temporal activation pattern from the slow cortical potentials. Next, the decoding accuracy of the indirectly decoded individual muscle activation through the decoded muscle synergies were assessed.

To examine the weight of each muscle decoder (W_{muscle}) based on those of the muscle synergy decoders (W_{syn}), a 300-dimensional weight of an individual muscle decoder was reconstructed as a linear combination of the weights of the muscle synergy decoders with non-negative coefficients (W_{muscle}', conceptual schema presented in Figure 6C). The non-negative least squares problem was solved by the "lsqnonneg" function in MATLAB. The similarity of the weights of the original and reconstructed individual muscle decoders (i.e., W_{muscle} and W_{muscle}', respectively) was evaluated using Pearson's *r,* calculated from the decoder data of all participants.

Contribution of each electrode to decoding

To evaluate the spatial contributions of cortical activity to predict muscle synergy activations, we calculated the contribution of each electrode from the weights of the decoding model as determined in a previous study (Chao et al., 2010):

$$\%T_k = \frac{\sum_{j=1}^{L}|w_{kj}|}{\sum_{i=1}^{N_{electrode}}\sum_{j=1}^{L}|w_{ij}|} \times 100; \quad (3)$$

for all *k* from 1 to $N_{electrode}$, where $\%T_k$ is the percentage contribution of each EEG electrode *k*.

In addition, we divided the electrodes into four major ROIs to examine the individual contribution of each area to the decoding. The ROIs were the frontal area (F3, F1, Fz, F2, F4, FC3, FC1, FCz, FC2, and FC4), central area (FC1, FCz, FC2, C3, C1, Cz, C2, C4, CP1, and CP2), lateral area (FC5, FC3, FC4, FC6, C5, C6, CP5, CP3, CP4, and CP6), and parietal area (CP3, CP1, CP2, CP4, P3, P1, Pz, P2, and P4). Using the same procedure as for the full electrodes, the decoding accuracy of each muscle synergy activation was separately calculated using the electrode set in each ROI.

Effects of amplitude normalization of EMG signals

To examine the effect of amplitude normalization of EMG signals on the decoding of muscle synergy activation, we also extracted muscle synergies from non-normalized EMG activity and performed decoding analyses using the muscle synergy activation. We performed the same procedures for muscle synergy extraction and activation decoding as those used those for muscle synergies extracted from normalized EMGs.

Effects of motion artifact in EEG

The spectra of the EEG signals were analyzed using the fast Fourier transform (FFT) via the fft function in Matlab. Default setting parameters of the fft function were used (FFT size was set to

the length of the EEG signal rounded up to the next power of two). The power spectra of EEGs, which are affected by motion artifact during walking, exhibit the power peaks around the stride and step frequencies due to head motion (Arad et al., 2018; Kline et al., 2015; Nathan and Contreras-Vidal, 2016). Therefore, we calculated the relative power between the peak power in frequency from the stride to step frequencies and the mean power in the delta band frequency (0.5−4.0 Hz) as a rough indicator of artifact size of each electrode. Then, relationships between the artifact size and electrode contribution to the decoding, defined by formula (3), were examined using Pearson's correlation coefficient in each muscle synergy decoder per participant.

Supplemental experiment

Three participants walked on a treadmill under the same experimental conditions used in the main experiment. In this supplemental experiment, we measured tri-axial head accelerations with a 1000 Hz sampling frequency in addition to obtaining EEG, EMG, and GRF data under the same data recording conditions. An accelerometer (Trigno Wireless System, DelSys Inc., Boston, MA, USA) was attached to the participant's forehead along the midline of the nose (Figure S7), as described in previous studies (Kline et al., 2015; Nathan and Contreras-Vidal, 2016), to measure the best estimate of the head acceleration without any interfering EEG recordings.

Using the same analyses performed for the main experiment data, we extracted muscle synergies from EMG signals and then performed the decoding analysis of muscle synergy activation from slow cortical potentials obtained from the EEG signals. The acceleration signals were band-pass filtered between 0.5−4 Hz with a Butterworth filter (fourth-order) to examine the effects of head acceleration on the slow cortical potentials of EEGs. Then, the acceleration

data were resampled at 100 Hz to match the sampling frequency for the slow cortical potentials. If the head acceleration affected the activation patterns of the slow cortical potentials, the two signals showed a correlation with the time lag, in which the head movement preceded the slow cortical potentials. Because movement artifacts are mainly caused by vertical head accelerations (Kline et al., 2015), we calculated the cross-correlation between the time series of vertical head accelerations and slow cortical potentials at each electrode. The maximum correlation between the vertical head accelerations and the slow cortical potentials were examined in a time lag range from -500 to 500 ms so as not to exceed the step duration (approximately 600—900 ms depending on the participants). Finally, we used Pearson's correlation to examine the relationships between the electrode contribution to the decoding and the maximum correlation of the cross-correlation analysis in all the electrodes in each muscle synergy decoder.

Quantification and statistical analysis

The differences between the overall correlation values (i.e., decoding accuracy) between the two types of decoders (muscle synergy decoder vs. individual muscle decoder) were assessed using two-tailed paired t-tests. In addition, the differences in decoding accuracy between each ROI and the full electrode set were compared using repeated measures one-way analysis of variance (ANOVA) test with multiple t-tests with FDR correction for each muscle synergy type. Before performing the t-test and ANOVA, the normality was tested and found using the Lilliefors test. For the statistical tests, the coefficient of determination values were transformed into Z-values using Fisher’s Z-transformation and the tests (i.e., t-test, ANOVA, multiple t-tests with

FDR correction) were conducted on the Fisher's Z-values. Statistical significance was set at $p < 0.05$.

Supplemental References

Arad, E., Bartsch, R.P., Kantelhardt, J.W., and Plotnik, M. (2018). Performance-based approach for movement artifact removal from electroencephalographic data recorded during locomotion. PloS One 13, e0197153.

Berger, D.J., Gentner, R., Edmunds, T., Pai, D.K., and d'Avella, A. (2013). Differences in adaptation rates after virtual surgeries provide direct evidence for modularity. J. Neurosci. 33, 12384-12394.

Bradberry, T.J., Gentili, R.J., and Contreras-Vidal, J.L. (2010). Reconstructing three-dimensional hand movements from noninvasive electroencephalographic signals. J. Neurosci. 30, 3432-3437.

Bulea, T.C., Prasad, S., Kilicarslan, A., and Contreras-Vidal, J.L. (2014). Sitting and standing intention can be decoded from scalp EEG recorded prior to movement execution. Front. Neurosci. *8*, 376.

Carmena, J.M., Lebedev, M.A., Crist, R.E., O'Doherty, J.E., Santucci, D.M., Dimitrov, D.F., Patil, P.G., Henriquez, C.S., and Nicolelis, M.A. (2003). Learning to control a brain–machine interface for reaching and grasping by primates. Plos Biol. 1, e42.

Chao, Z.C., Nagasaka, Y., and Fujii, N. (2010). Long-term asynchronous decoding of arm motion using electrocorticographic signals in monkeys. Front. Neuroeng. 3, 3.

Clark, D.J., Ting, L.H., Zajac, F.E., Neptune, R.R., and Kautz, S.A. (2010). Merging of healthy motor modules predicts reduced locomotor performance and muscle coordination complexity post-stroke. J. Neurophysiol. 103, 844-857.

Contreras-Vidal, J.L., Bortole, M., Zhu, F., Nathan, K., Venkatakrishnan, A., Francisco, G.E., Soto, R., and Pons, J.L. (2018). Neural decoding of robot-assisted gait during rehabilitation after stroke. Am. J. Phys. Med. Rehabil. *97*, 541-550.

Corey, D.M., Dunlap, W.P., and Burke, M.J. (1998). Averaging correlations: Expected values and bias in combined Pearson rs and Fisher's z transformations. J. Gen. Psychol. 125, 245-261.

d'Avella, A., and Bizzi, E. (2005). Shared and specific muscle synergies in natural motor behaviors. Proc. Natl. Acad. Sci. U. S. A. 102, 3076-3081.

d'Avella, A., Portone, A., Fernandez, L., and Lacquaniti, F. (2006). Control of fast-reaching movements by muscle synergy combinations. J. Neurosci. 26, 7791-7810.

Delorme, A., and Makeig, S. (2004). EEGLAB: an open source toolbox for analysis of single-trial EEG dynamics including independent component analysis. J. Neurosci. Methods 134, 9-21.

Dominici, N., Ivanenko, Y.P., Cappellini, G., d'Avella, A., Mondi, V., Cicchese, M., Fabiano, A., Silei, T., Di Paolo, A., Giannini, C*., et al.* (2011). Locomotor primitives in newborn babies and their development. Science 334, 997-999.

Frere, J., and Hug, F. (2012). Between-subject variability of muscle synergies during a complex motor skill. Front. Comput. Neurosci. 6, 99.

Kline, J.E., Huang, H.J., Snyder, K.L., and Ferris, D.P. (2015). Isolating gait-related movement artifacts in electroencephalography during human walking. J. Neural Eng. 12, 046022.

Lee, D.D., and Seung, H.S. (1999). Learning the parts of objects by non-negative matrix factorization. Nature 401, 788-791.

Mullen, T.R., Kothe, C.A., Chi, Y.M., Ojeda, A., Kerth, T., Makeig, S., Jung, T.-P., and Cauwenberghs, G. (2015). Real-time neuroimaging and cognitive monitoring using wearable dry EEG. IEEE Trans. Biomed. Eng. *62*, 2553-2567.

Nakanishi, Y., Yanagisawa, T., Shin, D., Kambara, H., Yoshimura, N., Tanaka, M., Fukuma, R., Kishima, H., Hirata, M., and Koike, Y. (2017). Mapping ECoG channel contributions to trajectory and muscle activity prediction in human sensorimotor cortex. Sci. Rep. 7, 45486.

Nathan, K., and Contreras-Vidal, J.L. (2016). Negligible motion artifacts in scalp electroencephalography (EEG) during treadmill walking. Front. Hum. Neurosci. 9, 708.

Nielsen, J., Petersen, N., and Ballegaard, M. (1995). Latency of effects evoked by electrical and magnetic brain stimulation in lower limb motoneurones in man. J. Physiol. 484, 791-802.

Presacco, A., Forrester, L.W., and Contreras-Vidal, J.L. (2012). Decoding intra-limb and inter-limb kinematics during treadmill walking from scalp electroencephalographic (EEG) signals. IEEE Trans. Neural. Syst. Rehabil. Eng. 20, 212-219.

Presacco, A., Goodman, R., Forrester, L., and Contreras-Vidal, J.L. (2011). Neural decoding of treadmill walking from noninvasive electroencephalographic signals. J. Neurophysiol. 106, 1875-1887.

Terao, Y., Ugawa, Y., Hanajima, R., Machii, K., Furubayashi, T., Mochizuki, H., Enomoto, H., Shiio, Y., Uesugi, H., and Iwata, N.K. (2000). Predominant activation of I1-waves from the leg motor area by transcranial magnetic stimulation. Brain Res. 859, 137-146.

Theiler, J., Eubank, S., Longtin, A., Galdrikian, B., and Farmer, J.D. (1992). Testing for nonlinearity in time series: the method of surrogate data. Phys. D *58*, 77-94.

Tibshirani, R., Walther, G., and Hastie, T. (2001). Estimating the number of clusters in a data set via the gap statistic. J. R. Statist. Soc. B *63*, 411-423.

Torres-Oviedo, G., Macpherson, J.M., and Ting, L.H. (2006). Muscle synergy organization is robust across a variety of postural perturbations. J. Neurophysiol. 96, 1530-1546.

Yokoyama, H., Hagio, K., Ogawa, T., and Nakazawa, K. (2017a). Motor module activation sequence and topography in the spinal cord during air-stepping in human: Insights into the traveling wave in spinal locomotor circuits. Physiol. Rep. 5, e13504.

Yokoyama, H., Ogawa, T., Kawashima, N., Shinya, M., and Nakazawa, K. (2016). Distinct sets of locomotor modules control the speed and modes of human locomotion. Sci. Rep. *6,* 36275.

Yokoyama, H., Ogawa, T., Shinya, M., Kawashima, N., and Nakazawa, K. (2017b). Speed dependency in α-motoneuron activity and locomotor modules in human locomotion: indirect evidence for phylogenetically conserved spinal circuits. Proc. R. Soc. B *284*, 20170290.